Available online at www.sciencedirect.com
SCIENCE DIRECT®
Journal of Sound and Vibration 290 (2006) 1141–1174
JOURNAL OF SOUND AND VIBRATION
www.elsevier.com/locate/jsvi

Positional FEM formulation for flexible multi-body dynamic analysis

M. Greco[a], H.B. Coda[b,*]

[a]*Civil Engineering Department, Federal University of Uberlandia, Brazil*
[b]*São Carlos School of Engineering, University of São Paulo, Brazil*

Received 29 October 2003; received in revised form 29 April 2005; accepted 7 May 2005
Available online 19 August 2005

Abstract

This paper presents a simple formulation to deal with flexible multi-body dynamic systems by the finite element method. The proposed methodology is based on the minimum potential energy theorem written regarding nodal positions. Velocity, acceleration and strain are achieved directly from positions, not displacements. A non-dimensional space is created and the relative curvature and fibers length are calculated for both reference and deformed configurations and used to calculate the strain energy at general points. The classical Newmark equations are used to integrate time. Damping is introduced into the mechanical system by a rheonomic energy functional. The final formulation has the advantage of being simple and easy to teach, when compared to classical counterparts. The behavior of a bench-mark problem (spin-up maneuver) is studied regarding the influence of mass representation on its overall transient and steady-state behavior. Three other examples are presented to show the applicability of the technique, namely, a flexible slider–crank mechanism, a flexible beam flight and a Peaucellier-type mechanism. The results are compared with other authors' numerical solutions.

1. Introduction

A great number of interesting researches have been developed regarding the transient dynamic analysis of flexible structures undergoing large motions. Simo and Vu Quoc's paper [1] describes

*Corresponding author. Tel.: +55 16 33739482; fax: +55 16 2739482.
E-mail addresses: mgreco@feciv.ufu.br (M. Greco), hbcoda@sc.usp.br (H.B. Coda).

0022-460X/$ - see front matter © 2005 Elsevier Ltd. All rights reserved.
doi:10.1016/j.jsv.2005.05.018

various different formulations for this purpose. The authors were interested mainly in the rotating beam stiffens due to inertial forces, proving that some previous formulations were unable to reproduce this important property. In that study three valid formulations were cited. The first one is the so-called corotational formulation, which uses a consistent linearization of the fully nonlinear beam theory. It makes use of a "floating frame" that accompanies the overall movement of the rotating bar. The strain measurement is of the second-order expansion, using the auxiliary floating frame as a reference, see Refs. [2,3].

The second one is called exact [1] and uses the fully nonlinear strain measurement. It also uses the floating frame as an intermediate reference, calculating the strains from this reference and then rotating them to the inertial reference. For both formulations the associated differential equation is achieved and afterwards the standard Galerkin approximation is employed to solve the problem.

The third formulation [4] employs a finite element procedure based on the theorem of minimum potential energy assuming a centerline elongation based on curvilinear coordinates and a first-order distortion. It is interesting to mention that the majority of dynamic nonlinear analyses is made following a corotational linearized procedure, where a floating frame reference is present [5–8].

The common point of all cited formulations is the intrinsic relation between strain and displacements, linearized or not, using a floating frame or curvilinear coordinates as a reference and considering the Timoshenko–Reissner hypothesis for the beam kinematics.

This study presents a simple formulation to deal with flexible multi-body dynamic systems (including the rotating beam) based on the principle of minimum potential energy. It is different from all other approaches as it is based on position description, not displacement, does not use a floating frame to define strain and adopts the Bernoulli hypothesis for beam kinematics.

The strain measurement used can be classified as the fully one, following [1], but is not written following the same steps of classical works, it uses simple formulas derived from undergraduate engineering textbooks. This engineering view will be emphasized here by calling the fully strain measurement *engineering nonlinear strain*. The choice for Bernoulli hypothesis, together with the engineering view of beams kinematics, makes the present formulation quite simple, resulting in an easy procedure to teach.

The paper also shows that adopting concentrated or distributed mass, with or without rotational inertia, has small importance in the overall behavior of the slender rotating beam problem, and that the proposed simple approach is able to capture all the desired effects when compared to the benchmark solution.

To solve the transient problem the Newmark time integrator scheme [9] is employed together with the proposed position description. Results show that the proposed formulation is suitable for dynamic geometrical nonlinear problems with large deflection and rotations, mainly for multi-body applications.

Section 2 describes an easy way to understand and compute the strain measurement. It presents the adopted approximation and the numerical calculations to achieve strain. Section 3 shows the nonlinear dynamic formulation based on the minimum potential energy theorem (written regarding nodal positions). Section 4 devotes special attention to the calculation of strain energy and its derivatives. It also describes the kinetic energy and its derivatives in order to built the nonlinear equilibrium equation and the numerical process of solution. In Section 5, for

completeness, the simple nodal member connection used to compose multi-body systems is shown. Section 6 presents four examples to demonstrate the accuracy and applicability of the formulation. The conclusions are presented in Section 7 and the references are listed at the end of the paper.

2. Adopted kinematics and strain calculation

A general configuration, "0" for initial or "A" for actual, of the center line of the frame element is written as a function of the nodal positions following, for instance, a cubic approximation for Y coordinates, regarding X coordinates.

Fig. 1 displays the nodal positions of node one $\left(X_1^{\Xi}, Y_1^{\Xi}, \theta_1^{\Xi}\right)$ or for node two $\left(X_2^{\Xi}, Y_2^{\Xi}, \theta_2^{\Xi}\right)$, where the symbol Ξ may assume "0" for initial configuration or "A" for actual configuration.

Writing y as a function of x gives a false impression that x is not a variable of the problem. In order to represent the studied body in a more suitable way, a non-dimensional space, represented by the variable ξ varying from 0 to 1, is created. Any pair $\left(x^0, y^0\right)$ for the initial position or $\left(x^A, y^A\right)$ for the actual one is written as a function of ξ, as follows:

$$x = X_1 + l_x \xi, \tag{1}$$

where

$$l_x = (X_2 - X_1), \tag{2}$$

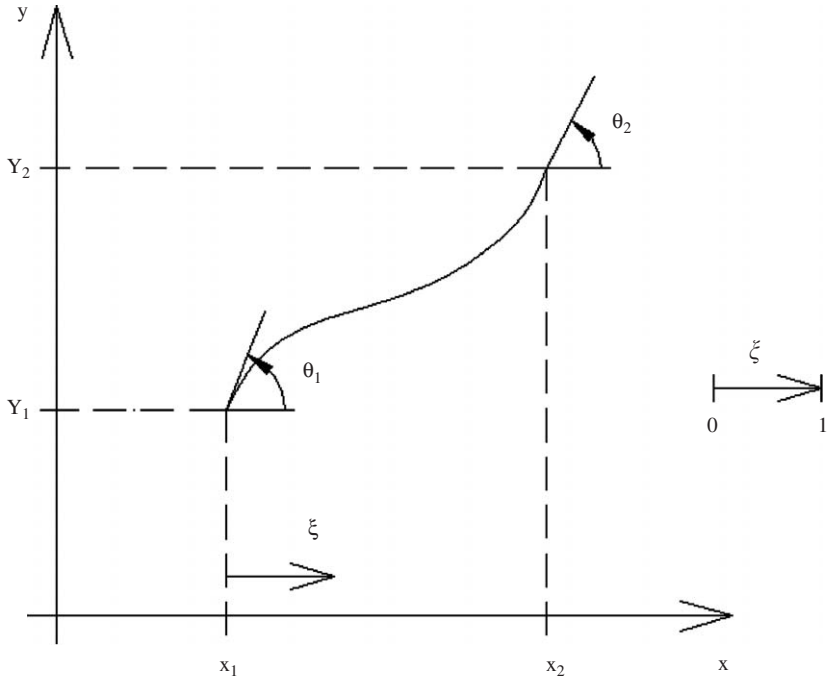

Fig. 1. Central line and nodal positions for both initial and actual configurations.

$$y = c\xi^3 + h\xi^2 + e\xi + f, \tag{3}$$

with

$$c = [tg(\theta_2) + tg(\theta_1)]l_x - 2l_y, \tag{4}$$

$$h = 3l_y - [tg(\theta_2) + 2tg(\theta_1)]l_x, \tag{5}$$

$$e = tg(\theta_1)l_x, \tag{6}$$

$$f = Y_1, \tag{7}$$

and

$$l_y = (Y_2 - Y_1). \tag{8}$$

It is important to note that for this approximation it is necessary to adjust the reference system to give $l_x \neq 0$. For any configuration, omitting symbol Ξ and following [10,11], the curvature written regarding the non-dimensional parameter ξ is

$$\frac{1}{r} = \frac{\frac{\mathrm{d}x}{\mathrm{d}\xi}\frac{\mathrm{d}^2y}{\mathrm{d}\xi^2}}{\left(\sqrt{\left(\frac{\mathrm{d}x}{\mathrm{d}\xi}\right)^2 + \left(\frac{\mathrm{d}y}{\mathrm{d}\xi}\right)^2}\right)^3}. \tag{9}$$

Or, replacing the given approximation, Eq. (3), results:

$$\frac{1}{r} = \frac{l_x(6c\xi + 2h)}{\left(\sqrt{l_x^2 + (3c\xi^2 + 2h\xi + e)^2}\right)^3}. \tag{10}$$

For slender bars, the Bernoulli hypothesis states that the plane cross-section remains plane and orthogonal to the central line of the bar after deformation. This hypothesis results in a proportional (longitudinal strain) to the curvature of the bar. It is also proportional to the orthogonal distance "z" (from the central line) of the considered point. Considering the non-dimensional space as an auxiliary reference, one writes

$$\varepsilon^{\Xi} = \left(\frac{1}{r}\right)^{\Xi} z. \tag{11}$$

Two additional considerations have to be made for expression (11). First the reference configuration must be the initial one, not the auxiliary one, resulting in

$$\varepsilon_{\text{bending}} = \varepsilon^A - \varepsilon^0 = \left[\left(\frac{1}{r}\right)^A - \left(\frac{1}{r}\right)^0\right] z. \tag{12}$$

The second consideration is that besides the bending strain, there is an elongation of the central line, so the total bending strain is rewritten as

$$\varepsilon_{\text{bending}} = \varepsilon_{\text{central}} + \left[\left(\frac{1}{r}\right)^A - \left(\frac{1}{r}\right)^0\right] z, \tag{13}$$

where $\varepsilon_{\text{central}}$ is the nonlinear engineering strain at the central line. Again, considering the auxiliary non-dimensional variable ξ it is possible to calculate the central strain as

$$\varepsilon_{\text{central}} = \frac{\mathrm{d}s^A - \mathrm{d}s^0}{\mathrm{d}s^0} = \frac{\frac{\mathrm{d}s^A}{\mathrm{d}\xi} - \frac{\mathrm{d}s^0}{\mathrm{d}\xi}}{\frac{\mathrm{d}s^0}{\mathrm{d}\xi}}, \tag{14}$$

where $\mathrm{d}s^0$ is the infinitesimal length of the initial central line and $\mathrm{d}s^A$ is the infinitesimal length of the central line for actual configuration. In this study, for simplicity, initially straight frame elements are adopted, so the necessary values to calculate the central strain are

$$\frac{\mathrm{d}s^0}{\mathrm{d}\xi} = \sqrt{\left(\frac{\mathrm{d}X_0}{\mathrm{d}\xi}\right)^2 + \left(\frac{\mathrm{d}Y_0}{\mathrm{d}\xi}\right)^2} = \sqrt{(l_{0x})^2 + (l_{0y})^2} = l_0, \tag{15}$$

where l_0 is the initial length of the finite element, and

$$\frac{\mathrm{d}s^A}{\mathrm{d}\xi} = \sqrt{\left(\frac{\mathrm{d}X^A}{\mathrm{d}\xi}\right)^2 + \left(\frac{\mathrm{d}Y^A}{\mathrm{d}\xi}\right)^2} = \sqrt{(l_x)^2 + \left(3c\xi^2 + 2h\xi + e\right)^2}. \tag{16}$$

Substituting Eqs. (15) and (16) in Eq. (14) results

$$\varepsilon_{\text{central}} = \frac{1}{l_0}\sqrt{(l_x)^2 + (3c\xi^2 + 2h\xi + e)^2} - 1. \tag{17}$$

Placing Eqs. (10), (13) and (17) together, and remembering that the initial configuration is a straight element, one has

$$\varepsilon_{\text{bending}} = \frac{1}{l_0}\sqrt{(l_x)^2 + (3c\xi^2 + 2h\xi + e)^2} - 1 + \frac{l_x(6c\xi + 2h)}{\left(\sqrt{l_x^2 + (3c\xi^2 + 2h\xi + e)^2}\right)^3} z, \tag{18}$$

where the constants c, h, e and l_x are written regarding the actual nodal positions $X_i = (X_1, Y_1, \theta_1, X_2, Y_2, \theta_2)$ and the values l_0 and z depend upon the initial geometry of the frame element. It is important to remember that the strain measurement is of the Lagrangian type and is similar to the fully strain measurement. The adopted kinematics is the Bernoulli one, which results in a different formulation when compared to the references.

3. Dynamic nonlinear formulation with damping (general aspects)

The conservation of energy in a mechanical system is guaranteed if the input and output of energy are at balance. If there is some kind of dissipation the total energy of the system changes along time. It can be understood writing the total potential energy of a system as follows:

$$\Pi = \Pi_0 - Q(t, x), \tag{19}$$

where $Q(t, x)$ can be stated as the quantity of energy withdrawn from the simple conservative idealized energy Π_0 [12]. Π is the remaining (actual) mechanical energy of the system. Eq. (19)

can be rewritten as

$$\Pi_0 = \Pi + Q(t, x). \tag{20}$$

This equation can be understood as recovering the possibility of using stationary properties for the mechanical system analysis, i.e., one can use the minimum potential energy theorem on the energy function Π_0 for equilibrium analysis.

For a structural problem associated with a fixed reference system, Fig. 2, the ideal potential energy function can be written as the composition of the strain energy (U_e), the potential energy of applied forces (P), the kinetic energy (K) and dissipation (Q), as follows.

$$\Pi_0 = U_e - P + K + Q. \tag{21}$$

The strain energy function of the body, frame for instance, is considered stored in the initial volume of the body (V_0) and is written as an integral of a specific strain energy value (u_e), as follows.

$$U_e = \int_{V_0} u_e \, \mathrm{d}V_0. \tag{22}$$

The strain energy is assumed to be zero in the initial position, called non-deformed. The adopted specific strain energy expression is given in Section 4. The potential energy of the applied conservative concentrated forces is written as

$$P = -F_i X_i, \tag{23}$$

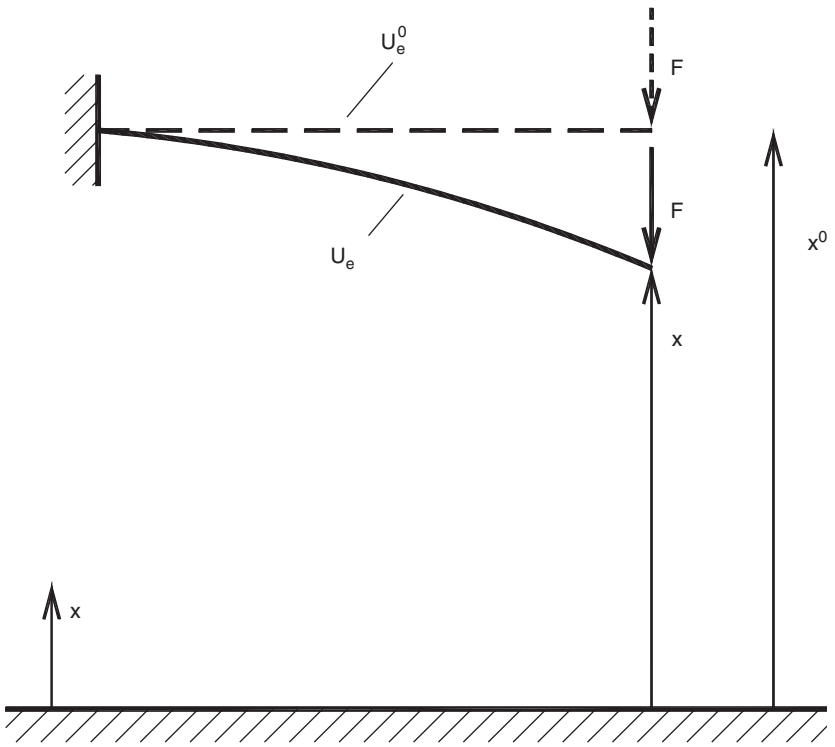

Fig. 2. Potential energy written for a structure in two different positions.

where F_i represents forces (or moments) applied in "i" direction and X_i is the ith coordinate parameter of the point where the load is applied. In this study distributed forces are not considered. The kinetic energy is given by

$$K = \frac{1}{2}\int_{V_0} \rho_0 \dot{x}_i \dot{x}_i \, \mathrm{d}V_0, \tag{24}$$

where $\dot{x}_i$ are velocities and ρ_0 is the mass density. The dissipative term is written in its differential form as

$$\frac{\partial}{\partial X_i} Q(t,x) = \int_{v_0} \frac{\partial}{\partial X_i} q(x,t) \, \mathrm{d}V_0 = \int_{v_0} \lambda_m \dot{x}_i \, \mathrm{d}V_0, \tag{25}$$

where q is the specific dissipative functional, λ_m is a proportionality constant and X_i is the position of any specific point (for FEM it is a nodal position).

It is interesting to observe that the potential energy of the applied forces may not be zero in the reference configuration. Substituting Eqs. (22)–(25) in Eq. (21) results in

$$\Pi_0 = \int_{V_0} u_e \, \mathrm{d}V_0 - F_i X_i + \frac{1}{2}\int_{V_0} \rho_0 \dot{x}_i \dot{x}_i \, \mathrm{d}V_0 + Q. \tag{26}$$

This energy function can be evaluated substituting the exact position field by its approximation described in Section 2, i.e.:

$$\Pi_0 = \int_{V_0} u_e(\xi, X_i) \, \mathrm{d}V_0 - F_i X_i + \frac{1}{2}\int_{V_0} \rho_0 \dot{x}_i^2(\xi, X_i) \, \mathrm{d}V_0 + Q(\xi, X_i). \tag{27}$$

The minimum potential energy theorem is used in Π_0, by differentiating Eq. (27) regarding a generic nodal position X_s, which results in

$$\frac{\partial \Pi_0}{\partial X_s} = \int_{V_0} \frac{\partial u_e(\xi, X_i)}{\partial X_s} \, \mathrm{d}V_0 - F_s + \int_{V_0} \rho_0 \dot{x}_i(\xi, X_i) \frac{\partial \dot{x}_i(\xi, X_i)}{\partial X_s} \, \mathrm{d}V_0 + \int_{V_0} \lambda_m \rho_0 \dot{x}_s(\xi, X_i) \, \mathrm{d}V_0 = 0. \tag{28}$$

In a vector form Eq. (28) is simply written as

$$g = \frac{\partial U_e}{\partial X_s} + F_{\text{inert.}} + F_{\text{damp.}} - F_{\text{ext}} = 0. \tag{29}$$

The vector of inertial force is $F_{\text{inert.}}$, the force due to damping is $F_{\text{damp.}}$ and the external force is $F_{\text{ext.}}$. The term $\frac{\partial U_e}{\partial X_s}$ is called here elastic internal force. It is important to remember that for Lagrangian description the mass and damping influences are integrated over the initial volume, as well as the derivative of strain energy. The size of the vectors is the number of degrees of freedom of the analyzed body, associated with parameters $X_s = (X_s, Y_s, \theta_s)$ of each node s. The necessary algebraic calculations for each term of Eq. (28) are performed in further sections.

The equilibrium equation (28) or (29) at an instant t is nonlinear regarding X_i. In order to solve it, a Taylor expansion regarding X_i is used as follows:

$$g(X_k + \Delta X_k) = g(X_k) + \frac{\partial g(X_k)}{\partial X_k} \Delta X_k + O^2 = 0. \tag{30}$$

Neglecting higher-order errors O^2 one writes

$$\Delta X_k = -\left(\frac{\partial g(X_k)}{\partial X_k}\right)^{-1} g(X_k) \tag{31}$$

with (for conservative loads)

$$\frac{\partial g}{\partial X_k} = \int_{V_0} \frac{\partial^2 u_e(\xi, X_i)}{\partial X_s \partial X_k}\, \mathrm{d}V_0 + \int_{V_0} \rho_0 \left(\frac{\partial \dot{x}_i(\xi, X_i)}{\partial X_k} \frac{\partial \dot{x}_i(\xi, X_i)}{\partial X_s} + \dot{x}_i(\xi, X_i) \frac{\partial^2 \dot{x}_i(\xi, X_i)}{\partial X_s \partial X_k} \right) \mathrm{d}V_0 + \int_{V_0} \lambda_m \rho_0 \frac{\partial \dot{x}_i(\xi, X_i)}{\partial X_k}\, \mathrm{d}V_0 = 0. \tag{32}$$

In expression (32), the first term, at the central expression, represents the Hessian matrix, called stiffness matrix for linear analysis. The mass characteristics of the body are present in the second term and the damping properties are in the last term. To solve Eq. (29) (or Eq. (28)) for a specific time step one calculates g for an arbitrary X_k (usually the last known one) using expression (29), calculates $\frac{\partial g}{\partial X_k}$ using relation (32) and ΔX_k using Eq. (31), updates X_k, returns to Eq. (29) and repeats all the procedure until ΔX_k could be neglected.

4. Dynamic nonlinear formulation with damping (practical procedure)

In this part of the paper, sections two and three are coupled, in order to solve numerically the studied dynamic nonlinear problem.

4.1. Strain energy, internal elastic forces and Hessian matrix

As previously mentioned, Eqs. (28), (29) and (32), the elastic internal force and the Hessian matrix are given by

$$F_{\mathrm{el}} = \frac{\partial U_e}{\partial X_i} = \int_{V_0} \frac{\partial u_e}{\partial X_i}\, \mathrm{d}V_0 = \int_{V_0} u_{e,i}\, \mathrm{d}V_0, \tag{33a}$$

$$H = \int_{V_0} \frac{\partial^2 u_e(\xi, X_s)}{\partial X_i \partial X_k}\, \mathrm{d}V_0 = \int_{V_0} u_{e,ik}\, \mathrm{d}V_0, \tag{33b}$$

where u_e is the specific (per unity of volume) strain energy and the comma means partial derivative. In order to calculate these quantities one defines specific strain energy for one-dimensional elasticity and Bernoulli hypothesis by

$$u_e = \frac{E}{2}(\varepsilon_{\mathrm{bending}})^2. \tag{34}$$

Substituting Eq. (18) into Eq. (34) and remembering the parametric approximation defined from Eqs. (1)–(8), in a compact form, one writes

$$u_e = T\left(\frac{\sqrt{B}}{l_0} - 1\right)^2 + FGB^{-3}, \tag{35}$$

where

$$T = \frac{EAl_0}{2} \tag{36}$$

$$F = \frac{EIl_0}{2}, \tag{37}$$

$$B = (l_x)^2 + S(\xi), \tag{38}$$

$$G = (l_x)^2 N(\xi), \tag{39}$$

$$S(\xi) = s^2(\xi), \tag{40}$$

$$s(\xi) = 3c\xi^2 + 2h\xi + e, \tag{41}$$

$$N(\xi) = n^2(\xi), \tag{42}$$

$$n(\xi) = 6c\xi + 2h. \tag{43}$$

From Eq. (35) one writes

$$u_{e,i} = \frac{T}{l_0^2}\left(1 - \frac{l_0}{\sqrt{B}}\right)B_{,i} + \frac{FBG_{,i} - 3FB_{,i}G}{B^4}, \tag{44}$$

$$u_{e,ik} = \frac{T}{l_0^2}\left[\frac{l_0 B_{,i}B_{,k}}{2B^{2/3}} + \left(1 - \frac{l_0}{\sqrt{B}}\right)B_{,ik}\right] + \frac{F}{B^5}\left[-3B\left(G_{,i}B_{,k} + G_{,k}B_{,i} + GB_{,ik}\right) + G_{,ik}B^2 + 12GB_{,i}B_{,k}\right]. \tag{45}$$

In order to complete the necessary values one calculates the following variables $B_{,i}$ $B_{,k}$ $B_{,ik}$ $G_{,i}$ $G_{,k}$ $G_{,ik}$, remembering that (1,2,3,4,5,6) = (X_1, Y_1, Θ_1, X_2, Y_2, Θ_2). To simplify the calculations one could note that

$$\frac{\partial}{\partial X_1} = -\frac{\partial}{\partial l_x}, \quad \frac{\partial}{\partial X_2} = \frac{\partial}{\partial l_x}, \quad \frac{\partial}{\partial Y_1} = -\frac{\partial}{\partial l_y}, \quad \frac{\partial}{\partial Y_2} = \frac{\partial}{\partial l_y}. \tag{46}$$

The following notation is adopted to develop a computational program:

$$\frac{\partial^2 N}{\partial l_x \partial l_y} = D2NLXLY, \quad \frac{\partial^2 N}{\partial l_x \partial \Theta_1} = D2NLXT1 \tag{47}$$

and

$$G_{,i} = Gi, \quad G_{,ik} = Gik. \tag{48}$$

The first derivatives of B and G are given explicitly in Table 1. The second derivatives are symmetric and therefore only their superior parts are shown in Table 2.

The values of Tables 1 and 2 will be numerically available from variables of the kind *D2NLXLX* presented in Table 3.

Table 1
First derivatives regarding nodal parameters

$B1 = -(2LX + DSLX)$	$G1 = -(2LXN + (LX)^2 DNLX)$
$B2 = -DSLY$	$G2 = -(LX)^2 DNLY$
$B3 = DST1$	$G3 = (LX)^2 DNT1$
$B4 = 2LX + DSLX$	$G4 = 2LXN + (LX)^2 DNLX$
$B5 = DSLY$	$G5 = (LX)^2 DNLY$
$B6 = DST2$	$G6 = (LX)^2 DNT2$

Table 2
Second derivatives regarding nodal parameters

$B11 = 2 + D2SLXLX$	$G11 = 2N + 4LXDNLX + (LX)^2 D2NLXLX$
$B12 = 2SLXLY$	$G12 = 2LXDNLY + (LX)^2 D2NLXLY$
$B13 = -D2SLXT1$	$G13 = -(2LXDNT1 + (LX)^2 D2NLXT1)$
$B14 = -B11$	$G14 = -G11$
$B15 = -B12$	$G15 = -G12$
$B16 = -D2SLXT2$	$G16 = -(2LXDNT2 + (LX)^2 D2NLXT2)$
$B22 = D2SLYLY$	$G22 = (LX)^2 D2NLYLY$
$B23 = -D2SLYT1$	$G23 = -(LX)^2 D2NLYT1$
$B24 = -B21$	$G24 = -G21$
$B25 = -B22$	$G25 = -G22$
$B26 = -D2SLYT2$	$G26 = -(LX)^2 D2NLYT2$
$B33 = D2ST1T1$	$G33 = (LX)^2 D2NT1T1$
$B34 = -B31$	$G34 = -G31$
$B35 = -B32$	$G35 = -G32$
$B36 = D2ST1T2$	$G36 = (LX)^2 D2NT1T2$
$B44 = -B41$	$G44 = G11$
$B45 = -B42$	$G45 = -G42$
$B46 = D2SLXT2$	$G46 = -G16$
$B55 = B22$	$G55 = G22$
$B56 = D2SLYT2$	$G56 = (LX)^2 D2NLYT2$
$B66 = D2ST2T2$	$G66 = (LX)^2 D2NT2T2$

In order to reduce the complexity of notation, one may use index $(1, 2, 3, 4)$ in place of $(LX, LY, T1, T2)$ by doing so, Table 3 is condensed to the following expression:

$$DS(i) = 2sDs(i), \quad DN(i) = 2nDn(i). \tag{49}$$

The second derivatives regarding nodal parameters can be written as

$$D2S(i,j) = 2Ds(i)Ds(j) + 2sD2s(i,j), \quad D2N(i,j) = 2Dn(i)Dn(j) + 2nD2n(i,j). \tag{50}$$

For example, if $i = 1$ and $j = 3$ one has $D2s(1,3) = D2sLXT1$.

Table 3
First derivatives regarding nodal parameters for functions S and N

$DSLX = 2sDsLX$	$DNLX = 2nDnLX$
$DSLY = 2sDsLY$	$DNLY = 2nDnLY$
$DST1 = 2sDsT1$	$DNT1 = 2nDnT1$
$DSLX = 2sDsT2$	$DNT2 = 2nDnT2$

Table 4
First derivatives of approximation 'constants' regarding nodal variables

$vc1 = \tan T1 + \tan gT2$	$vh1 = -(2\tan T1 + \tan gT2)$	$ve1 = \tan T1$
$vc2 = -2$	$vh2 = 3$	$ve2 = 0$
$vc3 = LX \sec^2 T1$	$vh3 = -2Lx \sec^2 T1$	$ve3 = LX \sec^2 T1$
$vc4 = LX \sec^2 T2$	$vh4 = -LX \sec^2 T2$	$ve4 = 0$

From expressions (41) and (43), variables $Ds(i)$, $Ds(j)$, and $Ds(I,j)$ can be found as

$$\frac{\partial s(t)}{\partial v_i} = Ds(i) = 3c_{,i}\xi^2 + 2h_{,i}\xi + e_{,i}, \tag{51}$$

$$\frac{\partial n(t)}{\partial v_i} = Dn(i) = 6c_{,i}\xi + 2h_{,i}, \tag{52}$$

$$\frac{\partial^2 s(t)}{\partial v_i \partial v_j} = D2s(i,j) = 3c_{,ij}\xi^2 + 2h_{,ij}\xi + e_{,ij}, \tag{53}$$

$$\frac{\partial^2 n(t)}{\partial v_i \partial v_j} = D2n(i,j) = 6c_{,ij}\xi + 2h_{,ij}, \tag{54}$$

where v_i represents variables $(LX, LY, T1, T2)$.

In order to complete the procedure it is necessary to calculate the derivatives of the 'constants' (in reality they are variables which depend on the nodal positions) of the approximations functions regarding the nodal parameters. Using $vci = c_{,i}$ and $d2cij = c_{,ij}$ and doing the same for 'h' and 'e', one has the values described in Tables 4 and 5.

4.2. The mass matrix

Three different mass matrices will be derived in this work in order to show the dependence of general problems regarding the mass approximation adopted.

Table 5
Second derivatives of approximation 'constants' regarding nodal variables

$d2c11 = 0$	$d2h11 = 0$	$d2e11 = 0$
$d2c12 = 0$	$d2h12 = 0$	$d2e12 = 0$
$d2c13 = \sec^2 T1$	$d2h13 = -2\sec^2 T1$	$d2e13 = \sec^2 T1$
$d2c14 = \sec^2 T2$	$d2h14 = -\sec^2 T2$	$d2e14 = 0$
$d2c21 = 0$	$d2h21 = 0$	$d2e21 = 0$
$d2c22 = 0$	$d2h22 = 0$	$d2e22 = 0$
$d2c23 = 0$	$d2h23 = 0$	$d2e23 = 0$
$d2c24 = 0$	$d2h24 = 0$	$d2e24 = 0$
$d2c31 = \sec^2 T1$	$d2h31 = -2\sec^2 T1$	$d2e31 = \sec^2 T1$
$d2c32 = 0$	$d2h32 = 0$	$d2e32 = 0$
$d2c33 = 2Lx \sec^3 T1 \text{ sen } T1$	$d2h33 = -4Lx \sec^3 T1 \text{ sen } T1$	$d2e33 = 2Lx \sec^3 T1 \sin T1$
$d2c34 = 0$	$d2h34 = 0$	$d2e34 = 0$
$d2c41 = \sec^2 T2$	$d2h41 = -\sec^2 T2$	$d2e41 = 0$
$d2c42 = 0$	$d2h42 = 0$	$d2e42 = 0$
$d2c43 = 0$	$d2h43 = 0$	$d2e43 = 0$
$d2c44 = 2Lx \sec^3 T2 \text{ sen } T2$	$d2h44 = -2Lx \sec^3 T2 \text{ sen } T2$	$d2e44 = 0$

4.2.1. Lumped mass matrix

The lumped mass matrix is characterized by concentrating the mass at the nodes of the element, so the approximation of variables (1)–(8) is not followed by mass distribution.

Expression (24) in this situation changes to

$$K = \frac{1}{2}\int_{V_0} \rho_0 \dot{x}_i \dot{x}_i \, \mathrm{d}V_0 = \frac{\rho_0 l_0}{4}\int_{A_0} (\dot{x}_i(z)\dot{x}_i(z))^{\text{node1}} \, \mathrm{d}A_0 + \frac{\rho_0 l_0}{4}\int_{A_0} (\dot{x}_i(z)\dot{x}_i(z))^{\text{node2}} \, \mathrm{d}A_0, \tag{55}$$

where A_0 is the cross-section area, considered constant along the element and z is the distance (orthogonal to the central line) of the considered point and the central line. The values $\dot{x}_i$ are the velocity in the ith direction at the cross-section, placed at each node. At nodes, the position and velocity of such points are

$$x_1 = x = X + z\sin(\Theta), \tag{56}$$

$$x_2 = y = Y + z(1 - \cos(\Theta)), \tag{57}$$

$$\dot{x}_1 = \dot{x} = \dot{X} + z\cos(\Theta)\dot{\Theta}, \tag{58}$$

$$\dot{x}_2 = \dot{y} = \dot{Y} + z\sin(\Theta)\dot{\Theta}. \tag{59}$$

Substituting these values into Eq. (55) one has

$$\begin{aligned} K = {} & \frac{\rho_0 l_0}{4} A_0 (\dot{X}_1)^2 + \frac{\rho_0 l_0}{4} I_0 \cos^2(\Theta_1)(\dot{\Theta}_1)^2 + \frac{\rho_0 l_0}{4} A_0 (\dot{X}_2)^2 + \frac{\rho_0 l_0}{4} I_0 \cos^2(\Theta_2)(\dot{\Theta}_2)^2 \\ & + \frac{\rho_0 l_0}{4} A_0 (\dot{Y}_1)^2 + \frac{\rho_0 l_0}{4} I_0 \sin^2(\Theta_1)(\dot{\Theta}_1)^2 + \frac{\rho_0 l_0}{4} A_0 (\dot{Y}_2)^2 + \frac{\rho_0 l_0}{4} I_0 \sin^2(\Theta_2)(\dot{\Theta}_2)^2. \end{aligned} \tag{60}$$

Eq. (60) is easily simplified to

$$K = \frac{\rho_0 l_0}{4} A_0 (\dot{X}_1)^2 + \frac{\rho_0 l_0}{4} I_0 (\dot{\Theta}_1)^2 + \frac{\rho_0 l_0}{4} A_0 (\dot{Y}_1)^2 + \frac{\rho_0 l_0}{4} A_0 (\dot{X}_2)^2 + \frac{\rho_0 l_0}{4} I_0 (\dot{\Theta}_2)^2 + \frac{\rho_0 l_0}{4} A_0 (\dot{Y}_2)^2. \tag{61}$$

From this equation one writes simply

$$M = \frac{\partial^2 K}{\partial X_k \partial X_s} = \frac{1}{2} \begin{bmatrix} \rho_0 A_0 l_0 & 0 & 0 & 0 & 0 & 0 \\ 0 & \rho_0 A_0 l_0 & 0 & 0 & 0 & 0 \\ 0 & 0 & \rho_0 I_0 l_0 & 0 & 0 & 0 \\ 0 & 0 & 0 & \rho_0 A_0 l_0 & 0 & 0 \\ 0 & 0 & 0 & 0 & \rho_0 A_0 l_0 & 0 \\ 0 & 0 & 0 & 0 & 0 & \rho_0 I_0 l_0 \end{bmatrix} \tag{62}$$

and

$$F_{\text{inert.}} = \frac{\partial K}{\partial X_s} = M \ddot{X}_s. \tag{63}$$

4.2.2. Consistent mass matrix for small rotations

Imagining a rotating frame, like in corotational formulations, it is possible to test the applicability of the linear consistent mass matrix for the adopted finite element, which is done considering $\sin(\theta) = \text{tg}(\theta) = \theta$ and $\cos(\theta) = 1$ for expressions (1)–(8). Following a similar procedure as the one described for concentrated mass one has

$$M = \frac{\partial^2 K}{\partial X_k \partial X_s} = \begin{bmatrix} \frac{\rho_0 A_0 l_0}{3} & 0 & 0 \\ 0 & \left(\frac{156\rho_0 A_0 l_0}{420} + \frac{12\rho_0 I_0}{10 l_0}\right) & \left(\frac{22\rho_0 A_0 (l_0)^2}{420} + \frac{\rho_0 I_0}{10}\right) \\ 0 & \left(\frac{22\rho_0 A_0 (l_0)^2}{420} + \frac{\rho_0 I_0}{10}\right) & \left(\frac{4\rho_0 A_0 (l_0)^3}{420} + \frac{\rho_0 I_0 l_0}{30}\right) \\ \frac{\rho_0 A_0 l_0}{6} & 0 & 0 \\ 0 & \left(\frac{54\rho_0 A_0 l_0}{420} - \frac{12\rho_0 I_0}{10 l_0}\right) & \left(\frac{13\rho_0 A_0 (l_0)^2}{420} + \frac{\rho_0 I_0}{10}\right) \\ 0 & \left(\frac{-13\rho_0 A_0 (l_0)^2}{420} + \frac{\rho_0 I_0}{10}\right) & \left(\frac{-13\rho_0 A_0 (l_0)^3}{420} + \frac{\rho_0 I_0 l_0}{30}\right) \end{bmatrix}$$

$$\begin{bmatrix}
\frac{\rho_0 A_0 l_0}{6} & 0 & 0 \\
0 & \left(\frac{54\rho_0 A_0 l_0}{420} - \frac{12\rho_0 I_0}{10 l_0}\right) & \left(\frac{-13\rho_0 A_0 (l_0)^2}{420} + \frac{\rho_0 I_0}{10}\right) \\
0 & \left(\frac{13\rho_0 A_0 (l_0)^2}{420} + \frac{\rho_0 I_0}{10}\right) & \left(\frac{-13\rho_0 A_0 (l_0)^3}{420} + \frac{\rho_0 I_0 l_0}{30}\right) \\
\frac{\rho_0 A_0 l_0}{3} & 0 & 0 \\
0 & \left(\frac{156\rho_0 A_0 l_0}{420} + \frac{12\rho_0 I_0}{10 l_0}\right) & \left(\frac{-22\rho_0 A_0 (l_0)^2}{420} + \frac{\rho_0 I_0}{10}\right) \\
0 & \left(\frac{-22\rho_0 A_0 (l_0)^2}{420} + \frac{\rho_0 I_0}{10}\right) & \left(\frac{4\rho_0 A_0 (l_0)^3}{420} + \frac{4\rho_0 I_0 l_0}{30}\right)
\end{bmatrix} \tag{64}$$

$$F_{\text{inert.}} = \frac{\partial K}{\partial X_s} = M\ddot{X}_s. \tag{65}$$

4.2.3. Consistent mass matrix for large rotations

From Bernoulli hypothesis one writes for any point of the element:

$$x = x_{\text{central}} + z\,\sin(\Theta), \tag{66}$$

$$y = y_{\text{central}} + z(1 - \cos(\Theta)), \tag{67}$$

$$\dot{x} = \dot{x}_{\text{central}} + z\,\cos(\Theta)\dot{\Theta}, \tag{68}$$

$$\dot{y} = \dot{y}_{\text{central}} + z\,\sin(\Theta)\dot{\Theta}. \tag{69}$$

Substituting these values into Eq. (55) and integrating regarding the cross-section results in

$$\begin{aligned} K &= \frac{\rho_0 A_0 l_0}{2}\int_{l_0} (\dot{x}_{\text{central}})^2\,\mathrm{d}\xi + \frac{\rho_0 A_0 l_0}{2}\int_{l_0} (\dot{y}_{\text{central}})^2\,\mathrm{d}\xi + \frac{\rho_0 I_0 l_0}{2}\int_{l_0} (\dot{\theta})^2\,\mathrm{d}\xi \\ &= K_1 + K_2 + K_3. \end{aligned} \tag{70}$$

The first term of Eq. (70) is easily integrated, giving

$$K_1 = \frac{\rho_0 A_0 l_0}{2}\left[\frac{1}{3}(\dot{X}_1)^2 + \frac{1}{6}\dot{X}_1\dot{X}_2 + \frac{1}{3}(\dot{X}_2)^2\right]. \tag{71}$$

In order to facilitate the mathematical procedure but keeping the rotating inertia contribution even for slender bars, one assumes a linear behavior for $\dot{\theta}$ along the bar resulting in

$$K_3 = \frac{\rho_0 I_0 l_0}{2}\left[\frac{1}{3}(\dot{\Theta}_1)^2 + \frac{1}{6}\dot{\Theta}_1\dot{\Theta}_2 + \frac{1}{3}(\dot{\Theta}_2)^2\right]. \tag{72}$$

To develop K_2 one writes the following relation from Eqs. (3) and (7)

$$\dot{y}_{\text{central}} = \dot{c}\xi^3 + \dot{d}\xi^2 + \dot{e}\xi + \dot{Y}_1. \tag{73}$$

The values of $\dot{c}$, $\dot{d}$ and $\dot{e}$ are calculated from Eqs. (4)–(6) as

$$\dot{c} = [(\sec^2\theta_1)\dot{\theta}_1 + (\sec^2\theta_2)\dot{\theta}_2]l_x + [tg\ \theta_1 + tg\ \theta_2]\dot{l}_x - 2\dot{l}_y, \tag{74}$$

$$\dot{d} = 3\dot{l}_y - [2(\sec^2\theta_1)\dot{\theta}_1 + (\sec^2\theta_2)\dot{\theta}_2]l_x - [2tg\ \theta_1 + tg\ \theta_2]\dot{l}_x, \tag{75}$$

$$\dot{e} = -(\sec^2\theta_1)\dot{\theta}_1 l_x + tg\ \theta_1 \dot{l}_x. \tag{76}$$

In this case, instead of starting from Eq. (24) one should use the developments performed to achieve expression (32), remembering that the considered terms only regard $\dot{y}_{\text{central}}$, as the others are considered in Eqs. (71) and (72). Following similar steps used to develop the kernels of the Hessian matrix one achieves the necessary kernels to built numerically the mass matrix, i.e.,

$$m_{ks} = \frac{\partial^2 K_2}{\partial X_s \partial X_k} = \rho_0 l_0 A_0 \int_0^1 \left(\frac{\partial \dot{y}_c(\xi, X_i)}{\partial X_k} \frac{\partial \dot{y}_c(\xi, X_i)}{\partial X_s} + \dot{y}(\xi, X_i) \frac{\partial^2 \dot{y}_c(\xi, X_i)}{\partial X_s \partial X_k} \right) \mathrm{d}\xi, \tag{77}$$

where index c is used to represent the central line.

Similar quantities, as depicted in Tables 1–5, are achieved and processed to produce the mass matrix dependent of positions. It is necessary to comment that Newmark time approximation is employed before performing the derivatives regarding nodal positions indicated in Eq. (77).

Deriving K_1 and K_3 regarding positions and performing the sum with terms of Eq. (77) results in

$$M = \frac{\partial^2 K}{\partial X_k \partial X_s} = \begin{bmatrix} m_{11} + \dfrac{\rho_0 A_0 l_0}{3} & m_{12} & m_{13} & m_{14} + \dfrac{\rho_0 A_0 l_0}{6} & m_{15} & m_{16} \\ m_{21} & m_{22} & m_{23} & m_{24} & m_{25} & m_{26} \\ m_{31} & m_{32} & m_{33} + \dfrac{\rho_0 I_0 l_0}{3} & m_{34} & m_{35} & m_{36} + \dfrac{\rho_0 I_0 l_0}{6} \\ m_{41} + \dfrac{\rho_0 A_0 l_0}{6} & m_{42} & m_{43} & m_{44} + \dfrac{\rho_0 A_0 l_0}{3} & m_{45} & m_{46} \\ m_{51} & m_{52} & m_{53} & m_{54} & m_{55} & m_{56} \\ m_{61} & m_{62} & m_{63} + \dfrac{\rho_0 I_0 l_0}{6} & m_{64} & m_{56} & m_{66} + \dfrac{\rho_0 I_0 l_0}{3} \end{bmatrix} \tag{78}$$

Internal forces are calculated by

$$F_{\text{inert.}} = \frac{\partial K}{\partial X_s} = M\ddot{X}_s. \tag{79}$$

4.3. Time marching process

From the previous developments Eq. (29) can be written as

$$f = \frac{\partial U_e}{\partial X} - F + M\ddot{X} + C\dot{X} = 0. \tag{80}$$

Expression (80) represents the dynamic equilibrium equation at any time and has to be solved. In order to do so the first step is to write this equilibrium for a specific instant (*S+1*), as follows:

$$\left.\frac{\partial \Pi}{\partial X}\right|_{S+1} = \left.\frac{\partial U_e}{\partial X}\right|_{S+1} - F_{S+1} + M\ddot{X}_{S+1} + C\dot{X}_{S+1} = 0. \tag{81}$$

Applying the Newmark β approximations for position description one has

$$X_{S+1} = X_S + \Delta t\dot{X}_S + \Delta t^2\left[\left(\frac{1}{2} - \beta\right)\ddot{X}_S + \beta\ddot{X}_{S+1}\right], \tag{82}$$

$$\dot{X}_{S+1} = \dot{X}_S + \Delta t(1-\gamma)\ddot{X}_S + \gamma\Delta t\ddot{X}_{S+1}. \tag{83}$$

Substituting approximations (82) and (83) into Eq. (81) results in

$$g(X_{S+1}) = \left.\frac{\partial \Pi}{\partial X}\right|_{S+1} = \left.\frac{\partial U_e}{\partial X}\right|_{S+1} - F_{S+1} + \frac{M}{\beta\Delta t^2}X_{S+1} - MQ_S + CR_S + \frac{\gamma C}{\beta\Delta t}X_{S+1} - \gamma\Delta t CQ_S = 0, \tag{84}$$

where vectors Q_S and R_S represent the dynamic contribution of the past, and are given by

$$Q_S = \frac{X_S}{\beta\Delta t^2} + \frac{\dot{X}_S}{\beta\Delta t} + \left(\frac{1}{2\beta} - 1\right)\ddot{X}_S, \tag{85}$$

$$R_S = \dot{X}_S + \Delta t(1-\gamma)\ddot{X}_S. \tag{86}$$

Eq. (84) can be understood simply by $g(X_{S+1}) = 0$ and is clearly nonlinear in (X_{S+1}). As described in Section 3, a Taylor expansion to solve this nonlinear equation regarding positions is applied, as follows:

$$\left.\frac{\partial^2 \Pi}{\partial X^2}\right|_{S+1} = \nabla g(X_{S+1}) = \left.\frac{\partial^2 U_e}{\partial X^2}\right|_{S+1} + \frac{M}{\beta\Delta t^2} + \frac{\gamma C}{\beta\Delta t}, \tag{87}$$

where C is assumed proportional to M, see Eq. (25). From Eq. (40) one builds the Taylor series of first order as

$$0 = g(X) \cong g\left(X^0\right) + \nabla g\left(X^0\right)\Delta X \tag{88}$$

and derives the Newton–Raphson procedure to solve the nonlinear Eq. (84), i.e.,

$$\nabla g\left(X^0\right)\Delta X = -g\left(X^0\right), \tag{89}$$

where X^0 is a trial position (usually X_s) for X_{S+1} used in Eq. (84) to calculate $g\left(X^0\right)$. Solving ΔX one calculates a new trial for X_{S+1} as

$$X_{S+1} = X^0 + \Delta X. \tag{90}$$

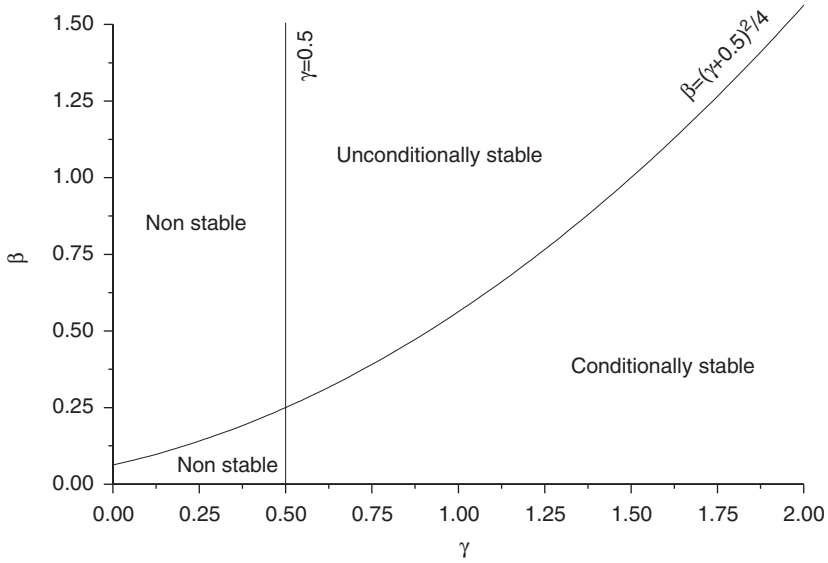

Fig. 3. Newmark parameters stability regions.

The acceleration must be corrected by an expression obtained from Eq. (82).

$$\ddot{X}_{S+1} = \frac{X_{S+1}}{\beta \Delta t^2} - Q_S. \tag{91}$$

This equation is used in Eq. (83) to correct velocity. The stop criterion is given in Eq. (92), when a chosen tolerance (TOL) is satisfied.

$$\left\| g(X^0) \right\| \leqslant \mathrm{TOL}. \tag{92}$$

It must be noted that, before the first time step, the initial acceleration must be calculated as follows

$$\ddot{X}_0 = M^{-1} \left[F_0 - \left. \frac{\partial U_e}{\partial X} \right|_0 - C\dot{X}_0 \right]. \tag{93}$$

The Newmark parameters (γ and β) can be chosen in order to achieve a stable algorithm, see Fig. 3 [9]. For instance, using constant acceleration for a time step ($\gamma = 0.50$ and $\beta = 0.25$) the unconditional stability is obtained.

5. Simple nodal member connection

This section presents an easy way to introduce free nodal degrees of freedom into 2D frame structures, i.e., articulated joints. This kind of connection is important for the analysis of mechanisms. The numerical modeling is achieved on the FEM and the nodal degree of freedom connection is done by kinetic compatibility.

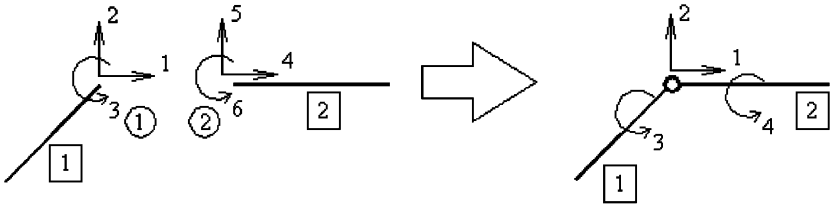

Fig. 4. Articulated joint degrees of freedom re-numbered.

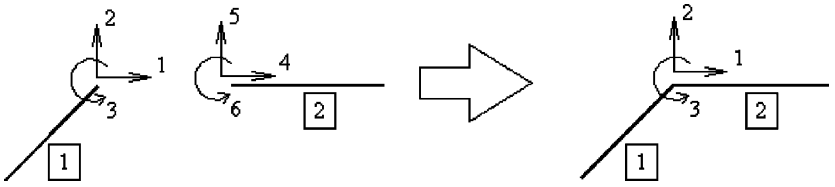

Fig. 5. Usual rigid nodal frame connection.

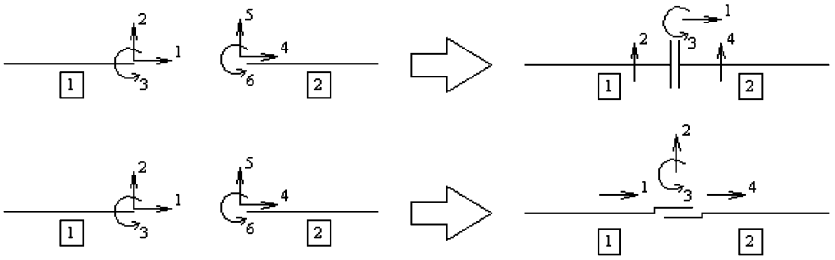

Fig. 6. Other nodal free movement connections.

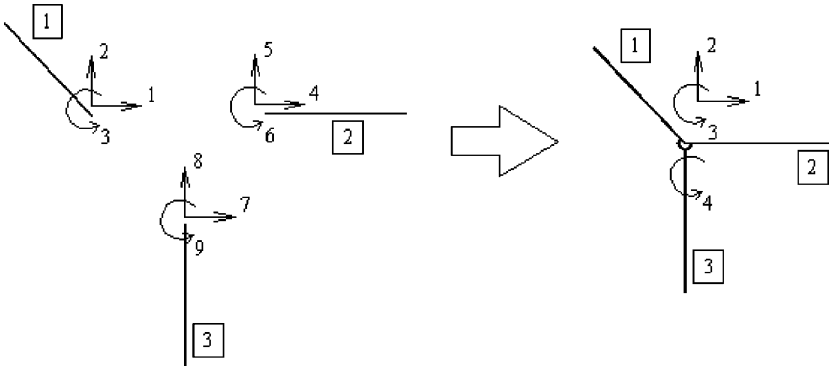

Fig. 7. Partial articulated joint between element 3 and the rigid sets 1–2.

The contribution of a single finite element matrix (Hessian, mass or damping) to the global matrix follows common degrees of freedom. The global degree of freedom k_{gl} of a node k cannot be given automatically by the formula $k_{\mathrm{gl}} = (3k - 1)$. A degree of freedom re-numbering is needed to build global matrices. For instance, in the case of an articulated joint, see Fig. 4, there are four degrees of freedom in the common node.

The uncoupled nodal matrices H have the following form:

$$H_1 = \begin{bmatrix} A_{11} & A_{12} & A_{13} \\ A_{12} & A_{22} & A_{23} \\ A_{13} & A_{23} & A_{33} \end{bmatrix}, \quad H_2 = \begin{bmatrix} B_{11} & B_{12} & B_{13} \\ B_{12} & B_{22} & B_{23} \\ B_{13} & B_{23} & B_{33} \end{bmatrix}. \tag{94}$$

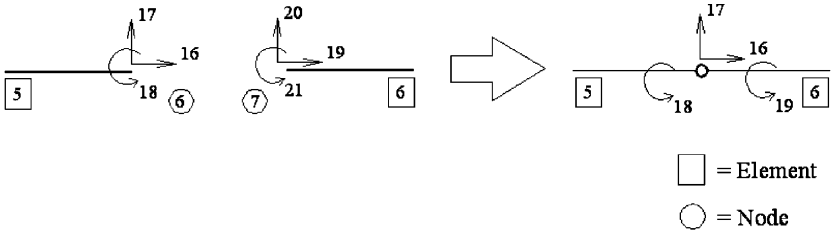

Fig. 8. Degrees of freedom re-numbering at the joint between the crank and connecting rod.

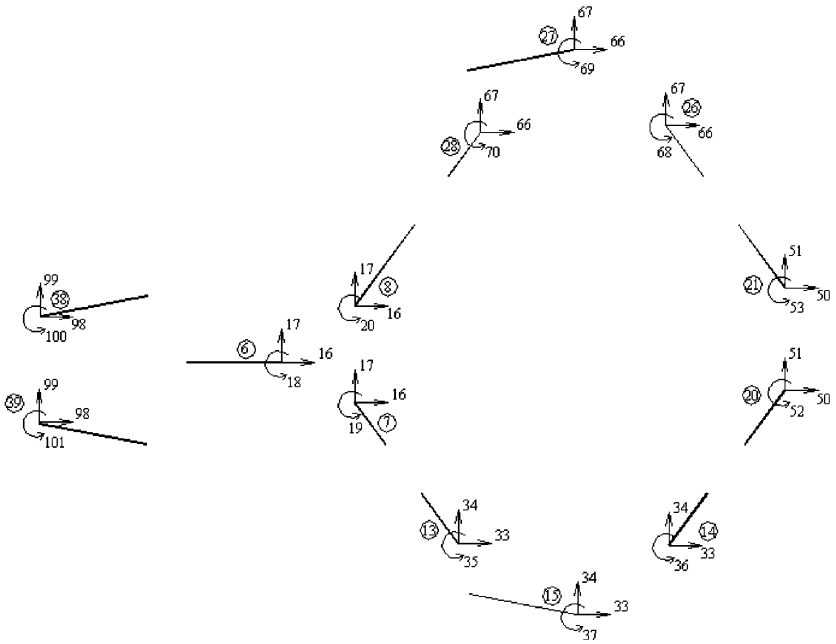

Fig. 9. Degrees of freedom re-numbering for the Peaucellier mechanism example.

The new coupled nodal matrix, after the connection, acquires the form

$$H = \begin{bmatrix} A_{11}+B_{11} & A_{12}+B_{12} & A_{13} & B_{13} \\ A_{12}+B_{12} & A_{22}+B_{22} & A_{23} & B_{23} \\ A_{13} & A_{23} & A_{33} & 0 \\ B_{13} & B_{23} & 0 & B_{33} \end{bmatrix}. \tag{95}$$

Instead, the usual rigid nodal frame connection has three degrees of freedom attached and does not need renumbering, as shown in Fig. 5.

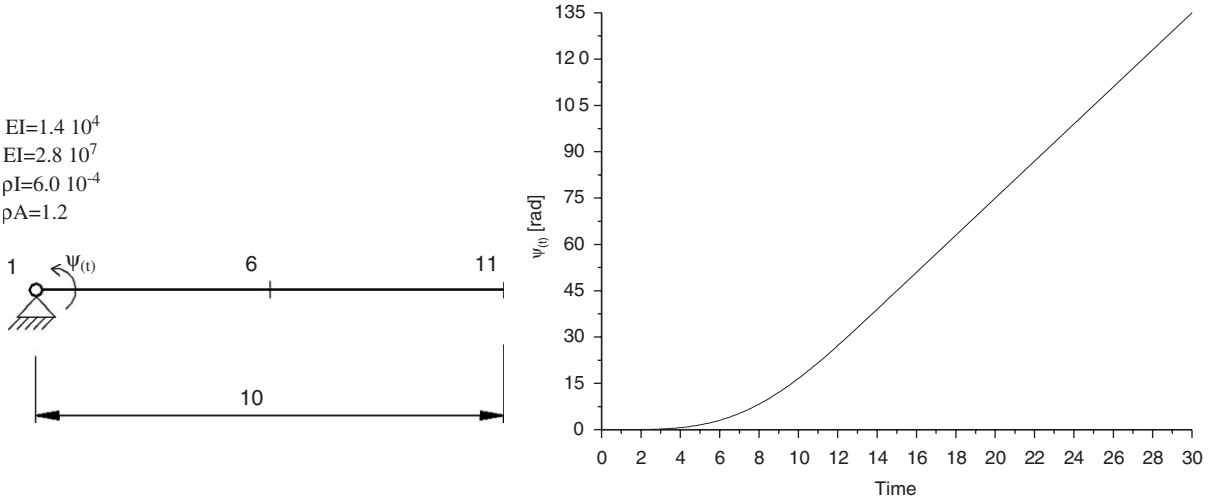

Fig. 10. Flexible spin-up maneuver input data.

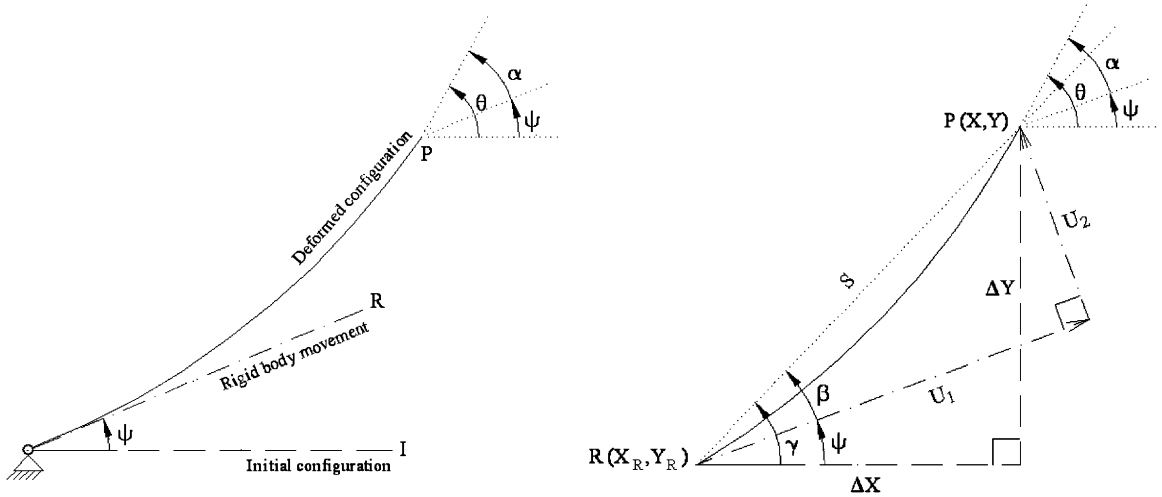

Fig. 11. Shape configurations and local system of coordinates.

Fig. 6 presents other types of re-numbering. It is also possible to have a partial nodal connection between one and more elements, as depicted in Fig. 7.

In Fig. 8 the re-numbering scheme used in example 3 is shown. In Fig. 9 the same is done for example 4.

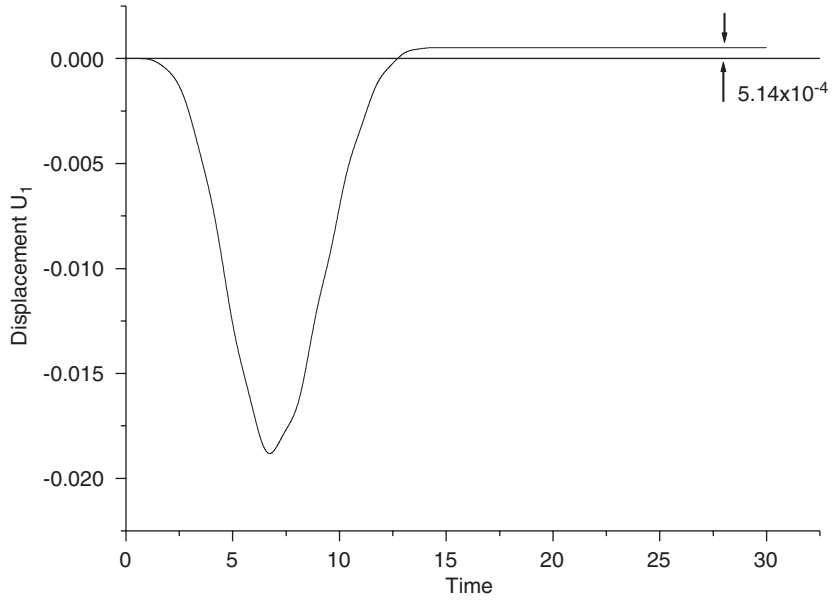

Fig. 12. Displacement U_1.

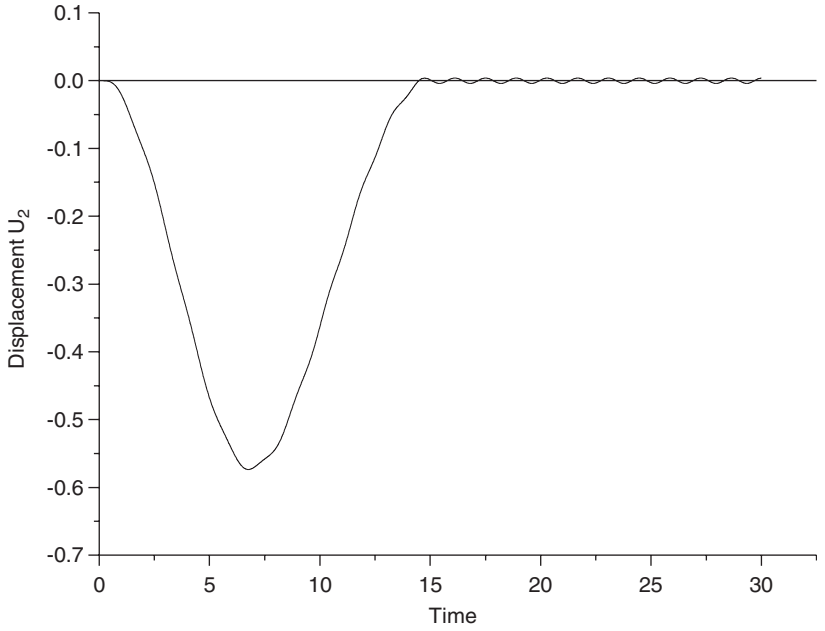

Fig. 13. Displacement U_2.

6. Numerical examples

This section provides some selected examples in order to verify the good behavior of the proposed formulation when dealing with general problems. It is important to note that the first

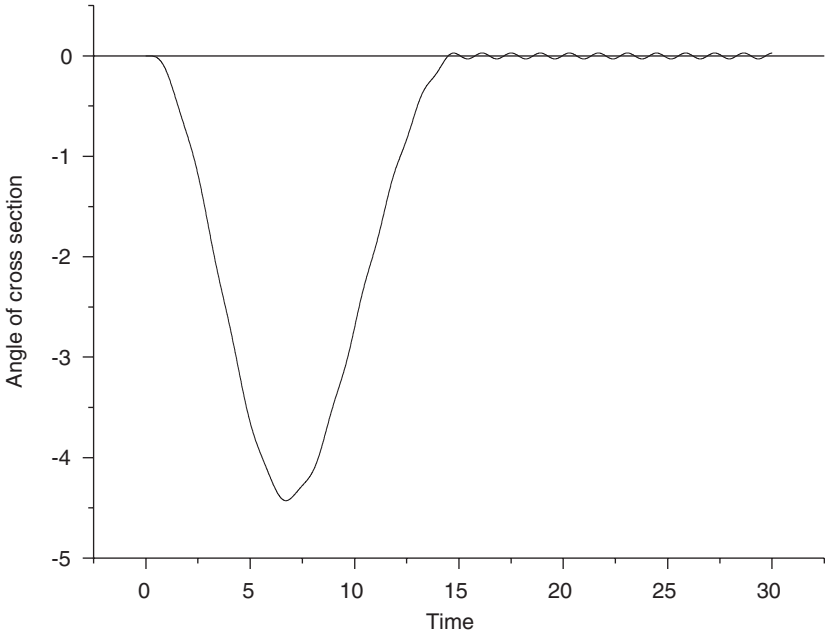

Fig. 14. Relative rotation angle α.

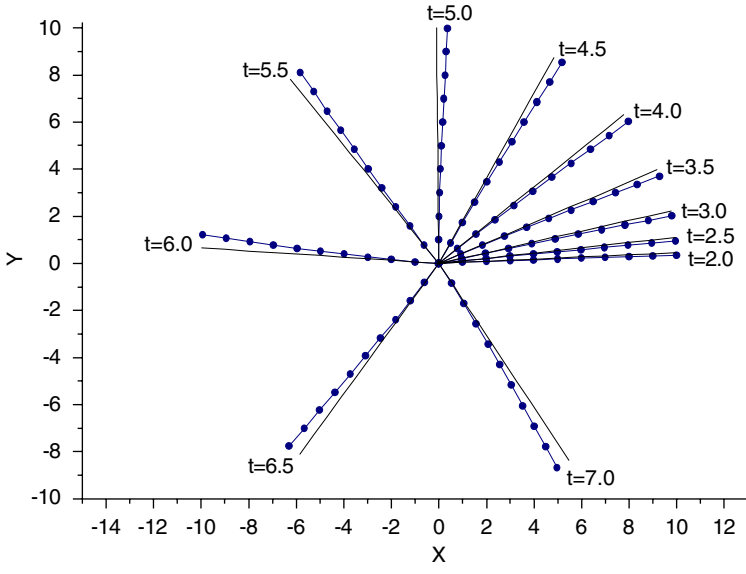

Fig. 15. Flexible beam, deformed shapes —■— and rigid body motions —, first cycle.

example is a benchmark of literature used to prove the capability of the proposed formulation to model all the necessary inertial characteristics of large rotation situations. We take the opportunity to show that, for slender bars, the rotational inertia of the cross-section is not

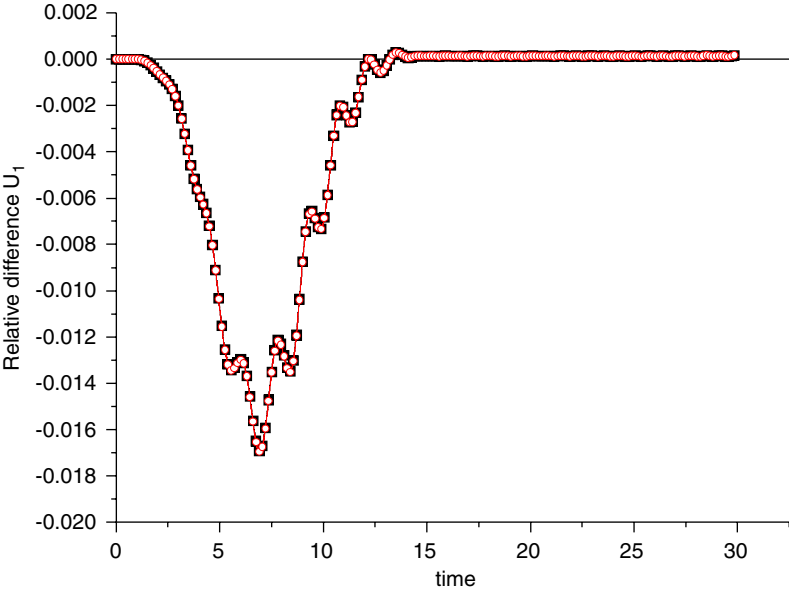

Fig. 16. Relative difference among solutions: complete solution —, concentrated mass without rotational inertia —■— and with rotational inertia —○—.

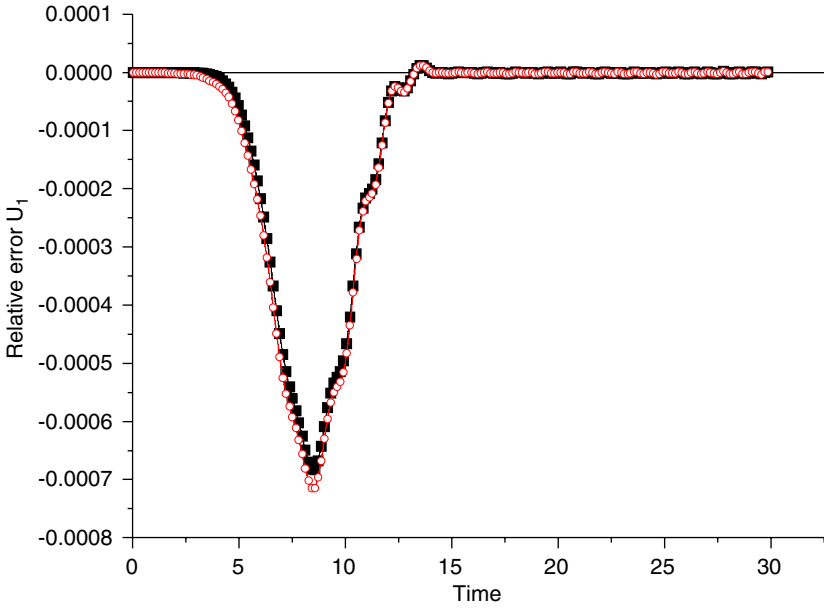

Fig. 17. Relative difference among solutions: complete solution —, linear (corotational) without rotational inertia —■— and with rotational inertia —○—.

important in the whole movement. The comparison between the results of concentrated mass and consistent linear mass distribution with the complete formulation also shows how the simplifications in the mass matrix influence the total behavior of the analyzed structure.

In the second example another benchmark problem is analyzed, where the member connection is used to model a slider–crank mechanism. In the third example *Simo's flexible beam in free flight* is modeled, showing the ability of the present formulation to analyze floating bodies developing finite deformations. In the last example a more complete mechanism is modeled to show the possibilities of the present formulation, including the mass proportional damping presented in the previous section.

6.1. Spin-up maneuver

The first numerical example is a simple fixed flexible beam and a benchmark of nonlinear dynamic formulations. It has been presented in several Refs. [3,8,13,14]. The spin-up maneuver is subject to a turn function ($\psi(t)$), applied on the restricted node, see Fig. 10. This type of turn function represents a typical helicopter blade rotation. The structure is approximated by a mesh of 10 finite elements. Several combinations of different mass matrices are tested in order to demonstrate that all effects, for this kind of analysis, have been captured.

The expressions of the turn function are presented in Eqs. (96) and (97).

$$\psi_{(t)} = \frac{2}{5}\left[\frac{t^2}{2} + \left(\frac{15}{2\pi}\right)^2\left(\cos\frac{2\pi t}{15} - 1\right)\right] \text{ rad}, \qquad 0 \leqslant t \leqslant 15, \tag{96}$$

$$\psi_{(t)} = (6t - 45) \text{ rad}, \qquad t > 15. \tag{97}$$

In Fig. 11, rigid body motion, initial and deformed configurations are presented. A local system of coordinates is created to compare results, where the displacements U_1 and U_2 are measured.

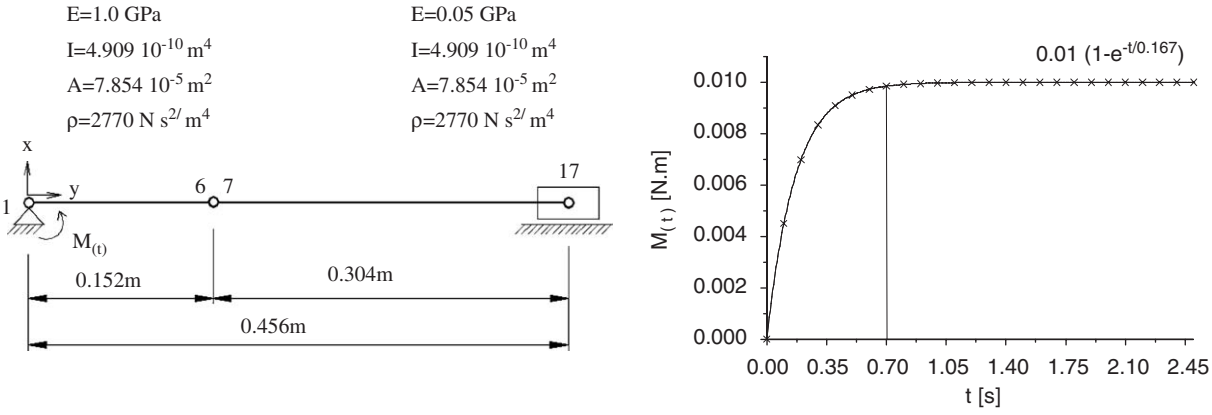

Fig. 18. Flexible mechanism input data: moment function 1 —×— and moment function 2 — .

From positions X and Y, and the rotation (θ) of the extreme node it is possible to calculate the displacements U_1 and U_2, and the relative rotation (α) between the deformed configuration and the rigid body motion, as follows.

$$S = \sqrt{\Delta X^2 + \Delta Y^2}, \tag{98}$$

$$\beta = \gamma - \psi, \tag{99}$$

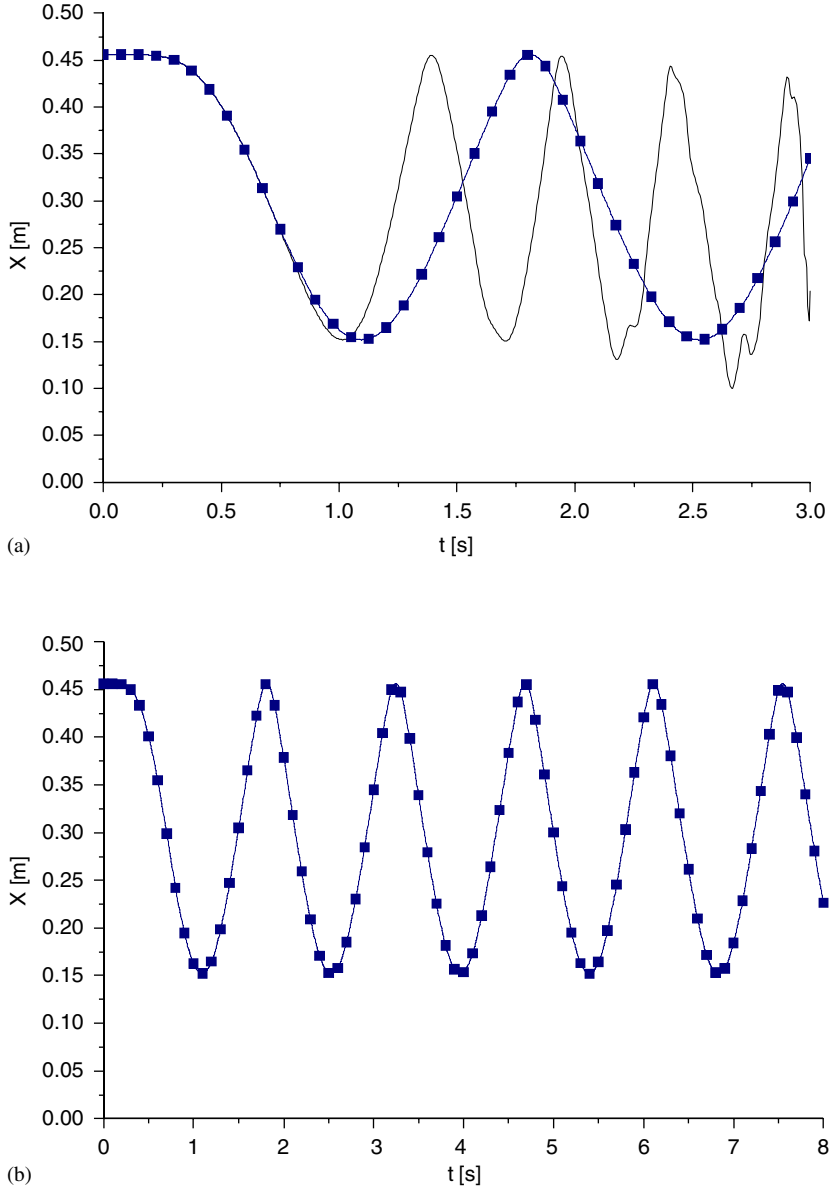

Fig. 19. (a) Block horizontal position (X) for the two moment functions: moment function 1 — , moment function 2 —■—. (b) Block horizontal position (X): moment function 2 —■—.

$$U_1 = S\cos\beta, \tag{100}$$

$$U_2 = S\sin\beta, \tag{101}$$

$$\alpha = \theta - \psi. \tag{102}$$

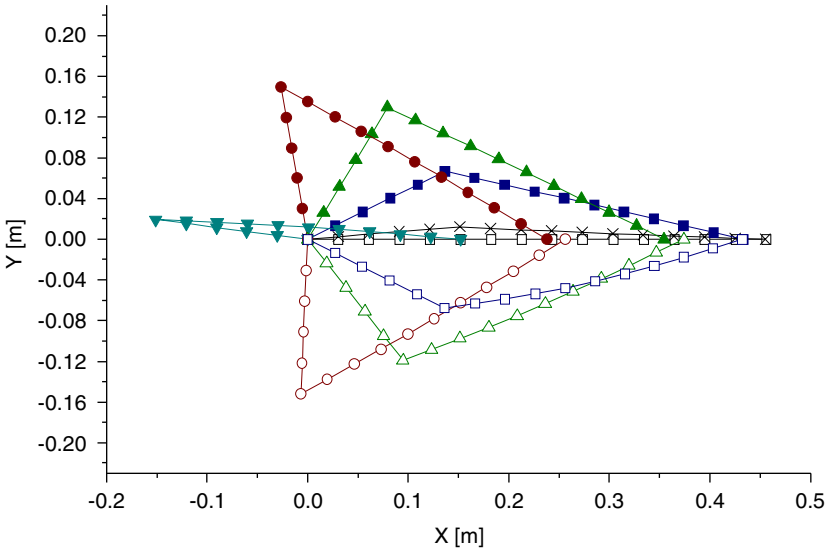

Fig. 20. Flexible mechanism deformed shapes for first moment function (first cycle) $t = 0.00$ s —□—, $t = 0.20$ s —×—, $t = 0.40$s —■—, $t = 0.60$ s —▲—, $t = 0.80$ s —●—, $t = 1.00$ s —▼—, $t = 1.20$ s —○—, $t = 1.30$ s —△—, $t = 1.35$ s —□—.

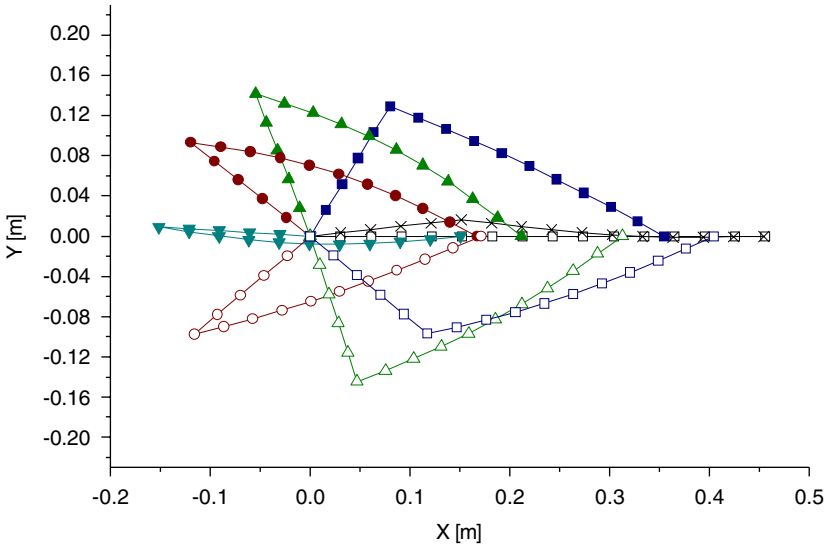

Fig. 21. Flexible mechanism deformed shapes for first moment function (second cycle) $t = 0.00$ s —□—, $t = 1.40$ s —×—, $t = 1.50$ s —■—, $t = 1.60$ s —▲—, $t = 1.65$ s —●—, $t = 1.70$ s —▼—, $t = 1.75$ s —○—, $t = 1.85$ s —△—, $t = 1.90$ s —□—.

Figs. 12–14 present displacements U_1 and U_2, and the relative rotation α, respectively, for the complete mass representation. Fig. 15 present the deformed shapes and the rigid body motions of the structure for some instants during the first cycle.

In Figs. 16 and 17 the longitudinal displacement differences among the response for different mass representations are shown. The relative difference is calculated referring to the maximum longitudinal displacement and considers the complete solution as the reference value. Two

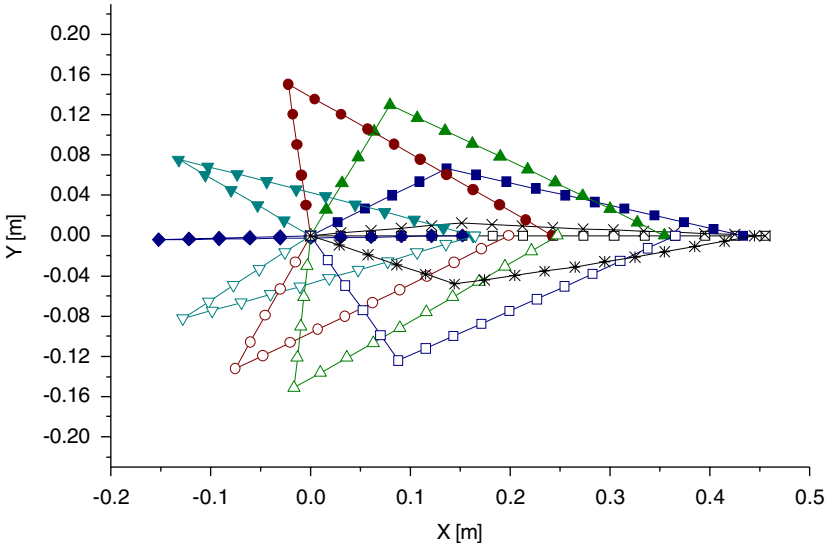

Fig. 22. Flexible mechanism deformed shapes for second moment function (first cycle) $t = 0.00$ s —□—, $t = 0.20$ s —×—, $t = 0.40$ s —■—, $t = 0.60$ s —▲—, $t = 0.80$ s —●—, $t = 1.00$ s —▼—, $t = 1.30$ s —○—, $t = 1.40$ s —△—, $t = 1.60$ s —□—.

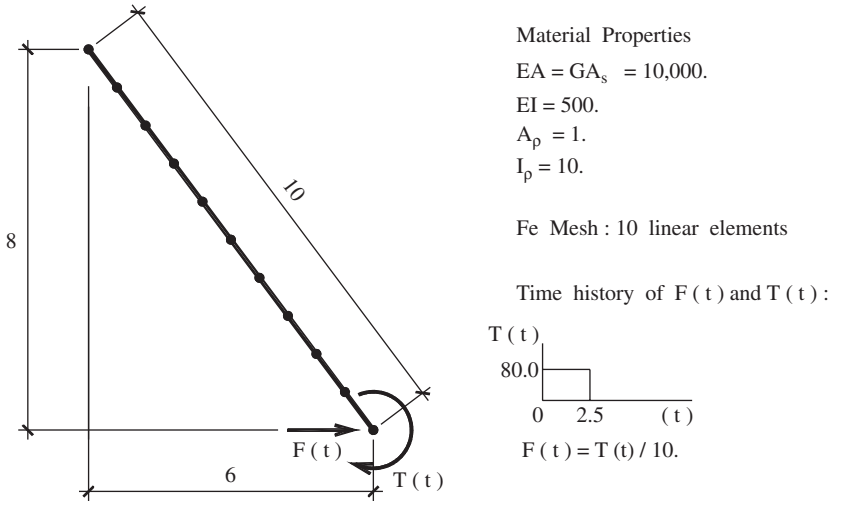

Fig. 23. Flexible beam in free flight, input data.

situations are considered for each comparison, with rotational inertia (WRI) and without rotational inertia (NRI).

There are non-perceptive differences (Figs. 12–15) between the results obtained and the ones found in Ref. [3]. One can see that the relative differences among the developed formulations are small. The concentrated mass presents a maximum difference of 1.8% regarding the complete formulation. As one can see the presence of rotational inertia (for cross-section) has almost no influence when slender bars are being considered.

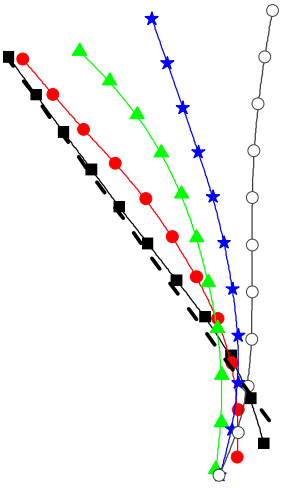

Fig. 24. Shapes for complete mass at instants: $t = 0.0\,\mathrm{s}$ – – –, $t = 0.5\,\mathrm{s}$ —■—, $t = 1.0\,\mathrm{s}$ —●—, $t = 1.5\,\mathrm{s}$ —▲—, $t = 2.0\,\mathrm{s}$ —★—, $t = 2.5\,\mathrm{s}$ —○—.

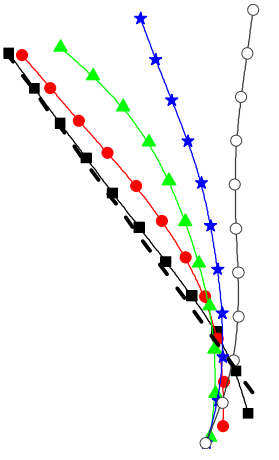

Fig. 25. Shapes for lumped mass at instants: $t = 0.0\,\mathrm{s}$ – – –, $t = 0.5\,\mathrm{s}$ —■—, $t = 1.0\,\mathrm{s}$ —●—, $t = 1.5\,\mathrm{s}$ —▲—, $t = 2.0\,\mathrm{s}$ —★—, $t = 2.5\,\mathrm{s}$ —○—.

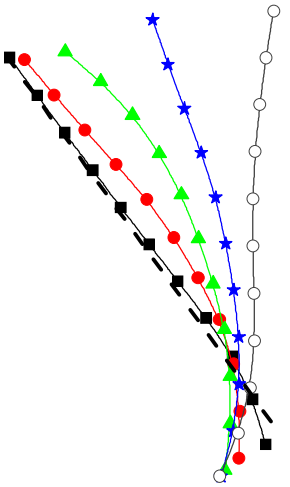

Fig. 26. Shapes for linear consistent (corotational) mass at instants: $t = 0.0$ s – – –, $t = 0.5$ s —■—, $t = 1.0$ s —●—, $t = 1.5$ s —▲—, $t = 2.0$ s —★—, $t = 2.5$ s —○—.

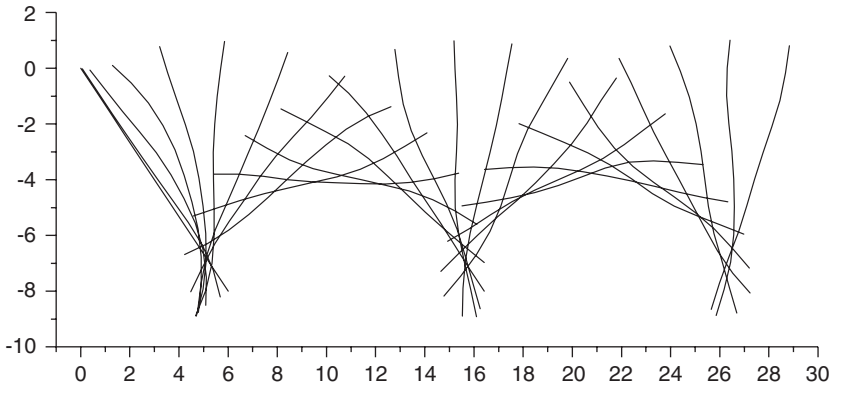

Fig. 27. Close up of the first two revolutions, positions.

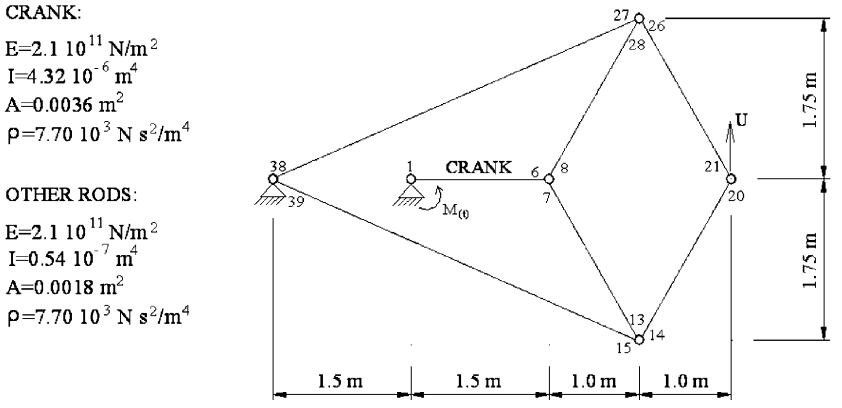

Fig. 28. Flexible Peaucellier mechanism input data.

6.2. Slider–crank mechanism

The second numerical example is a flexible slider–crank mechanism subject to a moment function ($M(t)$) applied on the crankshaft, see Fig. 18. Eqs. (103)–(105) present two different functions for $M_{(t)}$. The connecting rod is more flexible than the crank and the slider block is assumed rigid and without mass. The crank is discretized with 5 finite elements and the connecting rod with 10 finite elements. This example is presented in Ref. [15].

The first moment function is an exponential function with asymptotic behavior in $M_{(t)} = 0.01$ Nm.

$$M_{(t)} = 0.01\left(1 - e^{\frac{-t}{0.167}}\right) \text{ Nm}. \tag{103}$$

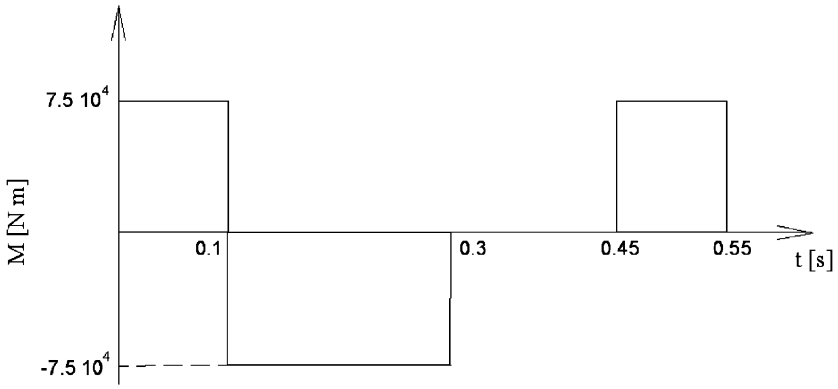

Fig. 29. Moment load data.

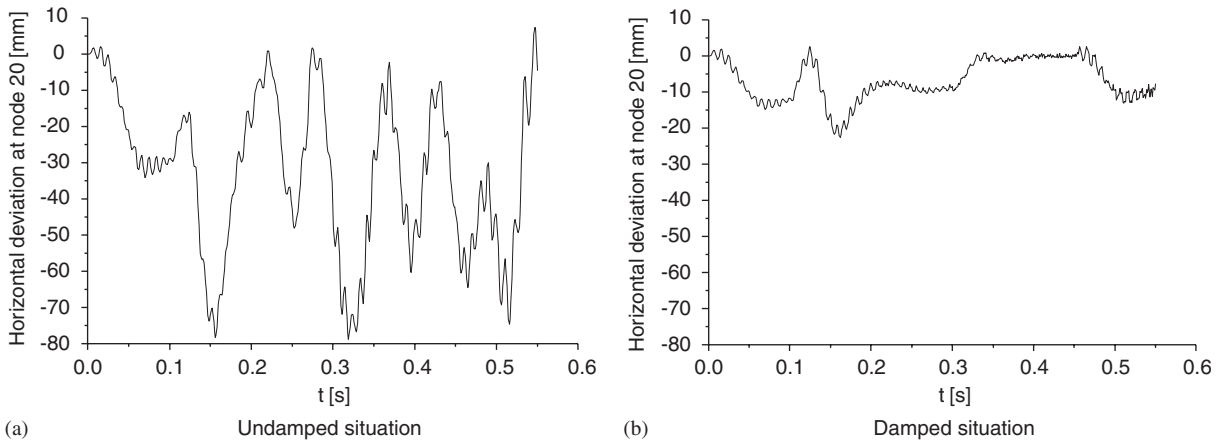

Fig. 30. Horizontal displacement for node *20*.

The second moment function has two phases, the first phase equal to Eq. (103) and the second phase equal to zero.

$$M_{(t)} = 0.01\left(1 - e^{\frac{-t}{0.167}}\right) \text{Nm}, \qquad 0s \leqslant t \leqslant 0.7 \text{ s}, \tag{104}$$

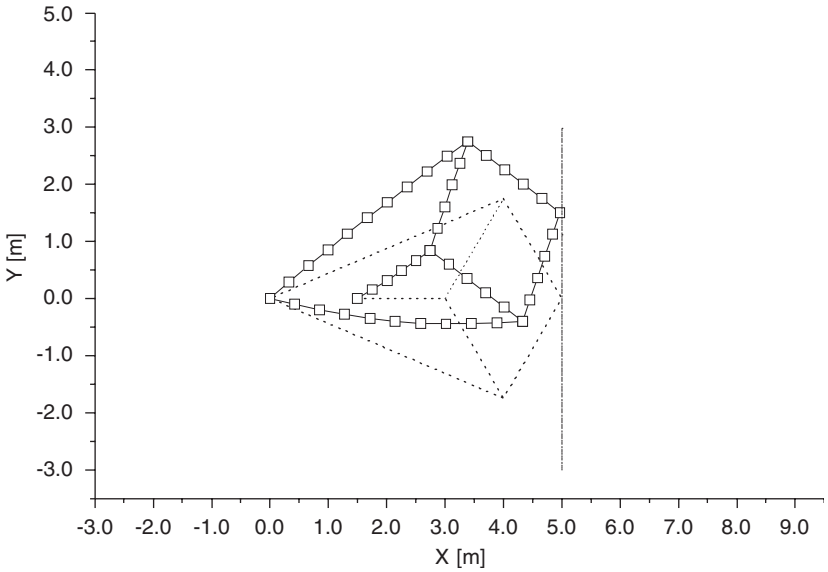

Fig. 31. Flexible mechanism deformation for time 0.106 s: initial shape - - - - -, node 20 rigid trajectory -·-·-·, flexible mechanism position —□—.

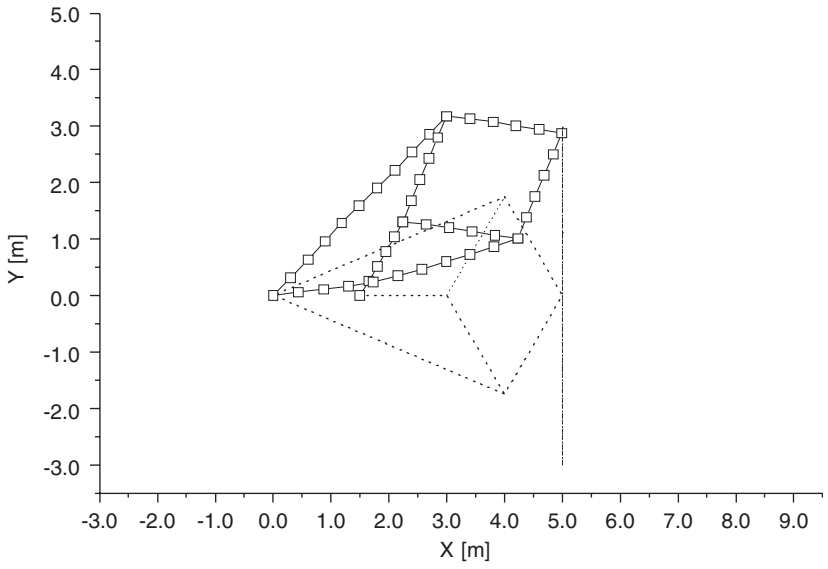

Fig. 32. Flexible mechanism deformation for time 0.212 s: initial shape, - - - - - node 20 rigid trajectory -·-·-·, flexible mechanism position —□—.

$$M_{(t)} = 0 \text{ Nm}, \qquad t > 0.7 \text{ s}. \tag{105}$$

In Fig. 19a positions X of the rigid block are presented for the two moment functions. In Fig. 19b the response to the second moment function, for a longer duration, is presented.

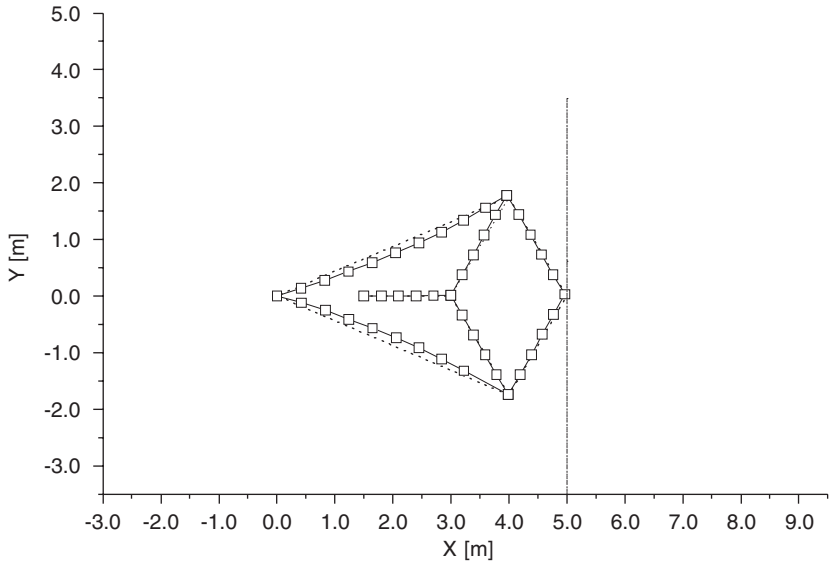

Fig. 33. Flexible mechanism deformation for instant 0.384 s: initial shape - - - - -, node 20 rigid trajectory ----·, flexible mechanism position —□—.

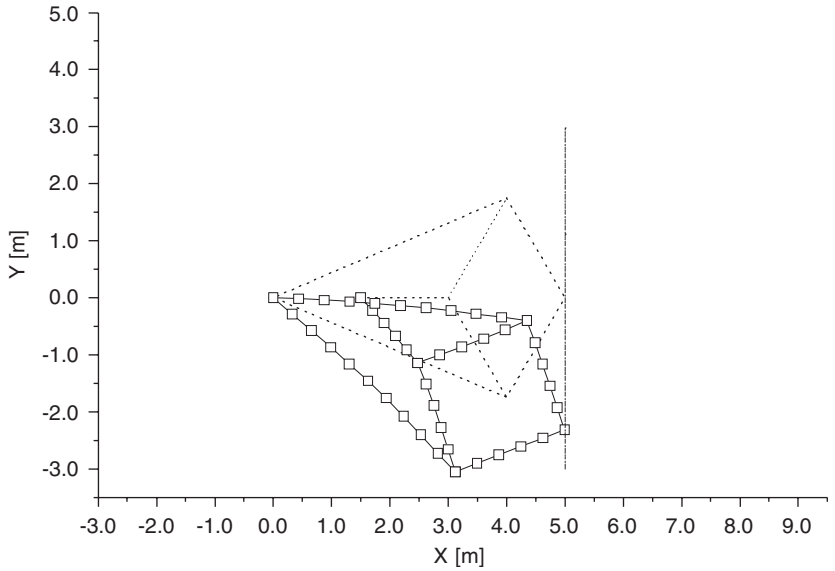

Fig. 34. Flexible mechanism deformation for instant 0.550 s: initial shape - - - - -, node 20 rigid trajectory ----·- flexible mechanism position —□—.

Some important values are compared with Ref. [15]. For the first moment function, the first minimum position time is 1.015 s for both present and referred works. The first maximum position time achieved by the present formulation is 1.390 s; the reference value is 1.395s. For the second moment function the first minimum position time achieved by the present formulation is 1.095 s and the reference value is 1.110 s. The first maximum instant for the proposed formulation is 1.810 s. Ref. [15] does not give the first maximum instant for this case.

Figs. 20 and 21 present the mechanism deformations for the first moment function considering the first and second cycles, respectively. The deformations due to the bending become clear after the second rotation cycle.

Fig. 22 presents the mechanism behavior for the second moment function, but just for the first rotation cycle. In this case, the movement is smoother, without initial oscillations generated by the deformations in the first moment function.

6.3. *Flexible beam in free flight*

Fig. 23 presents the geometry, physical properties and the applied loading of the flying beam. The stiffness of the beam is low enough to exhibit finite deformations. The motion of the beam during the load application is shown in Figs. 24–26, where the complete, lumped and linear consistent masses are respectively considered.

In Fig. 27 a close up of the first two revolutions is shown. The results are in total agreement with Ref. [3], a complete study using Reissner kinematics.

6.4. *Peaucellier mechanism*

The fourth numerical example is a Peaucellier mechanism [16]. The structure presented in Fig. 28 is divided into 45 finite elements. The number of elements adopted for each member can be identified in Fig. 28. When the members are considered rigid, node *20* presents a vertical straightline trajectory. The main objective of this example is to analyze the horizontal deviations that occur at node *20* when a flexible mechanism is considered. The moment load applied on the crank at node *1* is shown in Fig. 29.

Fig. 30 presents the horizontal deviation at node *20* and Figs. 26–29 present the flexible mechanism behavior. The achieved values of deviations are obviously unacceptable in machines designed to work with small geometrical tolerances. The proposed formulation can be useful to design this kind of machine considering admissible deviations. As expected, the viscosity reduces deviations and can be considered in the analysis by the proposed formulation. For this analysis the adopted damping parameter is $\lambda = 20\,\mathrm{day}^{-1}$.

Figs. 31–34 show the deformed positions of the studied mechanism.

7. Conclusions

A new, simple and accurate formulation to solve dynamic geometrical nonlinear problems with large deflections applied to multi-body analysis has been proposed. The formulation is based on position description, simplifying the understanding and the implementation of large deflection

analysis when compared with typical FEM formulations. The Newmark time integrator scheme has been successfully applied to integrate positions along time. An explanatory section regarding the way followed to consider free joints for multi-body plane analysis was given. Four examples were shown demonstrating the accuracy and possibilities of the formulation, mainly for multi-body applications. The influence of different mass matrix approaches has also been provided, showing that the overall structural behavior is slightly affected by mass considerations when slender bars are considered.

Acknowledgements

The authors would like to acknowledge FAPESP (Fundação de Amparo à Pesquisa do Estado de São Paulo) for the financial support given to this research.

References

[1] J.C. Simo, L. Vu-Quoc, The role of non-linear theories in transient dynamic analysis of flexible structures, *Journal of Sound and Vibration* 119 (1987) 487–508.
[2] J.C. Simo, L. Vu-Quoc, On the dynamics of flexible beams under large overall motions—the plane case—part 1, *Journal of Applied Mechanics, ASME* 53 (1986) 849–854.
[3] J.C. Simo, L. Vu-Quoc, On the dynamics of flexible beams under large overall motions—the plane case—part 2, *Journal of Applied Mechanics, ASME* 53 (1986) 855–863.
[4] T.R. Kane, R.R. Ryan, A.K. Banerjee, Dynamic of a beam attached to a moving base, *Astrodynamic Specialist Conference* (1986) AAS, 85–390.
[5] P. Wriggers, J.C. Simo, A general procedure for the direct computation of turning and bifurcation points, *International Journal for Numerical Methods in Engineering* 30 (1990) 155–176.
[6] M.A. Crisfield, A consistent corotational formulation for nonlinear, 3-dimensional, beam-elements, *Computer Methods in Applied Mechanics and Engineering* 81 (1990) 131–150.
[7] M.A. Crisfield, *Non-Linear Finite Element Analysis of Solids and Structures*, Vol. 1, Wiley, England, 1991.
[8] H.A. Elkaranshawy, M.A. Dokainish, Corotational finite element analysis of planar flexible multibody systems, *Computer & Structures* 54 (1995) 881–890.
[9] J. Argyris, H.P. Mlejnek, Dynamics of Structures, Texts on Computational Mechanics, Vol. 5, North-Holland, Amsterdam, 1991.
[10] C.R. Wylie, L.C. Barrett, *Advanced Engineering Mathematics*, sixth ed., McGraw-Hill, New York, 1995.
[11] H.B. Coda, M. Greco, A simple FEM formulation for large deflection 2D frame analysis based on position description, *Computer Methods in Applied Mechanics and Engineering* 193 (2004) 3541–3557.
[12] C. Lanczos, *The variational principles of mechanics*, fourth ed., Dover, New York, 1970.
[13] K.M. Hsiao, R.T. Yang, A.C. Lee, A consistent finite element formulation for non-linear dynamic analysis of planar beam, *International Journal for Numerical Methods in Engineering* 37 (1994) 75–89.
[14] E.R. Christensen, S.W. Lee, Nonlinear finite element modeling of the dynamics of unrestrained flexible structures, *Computer & Structures* 23 (1986) 819–829.
[15] J.L. Escalona, H.A. Hussein, A.A. Shabana, Application of the absolute nodal co-ordinate formulation to multibody system dynamics, *Journal of Sound and Vibration* 214 (1998) 833–851.
[16] A.A. Shabana, *Computational Dynamics*, Wiley, New York, 1994.